Simulation of Dynamical Processes in Molecular Solids

MICHAEL L. KLEIN

Department of Chemistry, University of Pennsylvania, Philadelphia, Pennsylvania 19104-6323

LAURENT J. LEWIS*

Département de Physique et Groupe de Recherche sur les Couches Minces, Université de Montréal, Case Postale 6128, Succursale A, Montréal, Québec H3C 3J7, Canada

Received October 9, 1989 (Revised Manuscript Received February 1, 1990)

Contents

Michael L. Klein received his B.Sc. (1961) and Ph.D. (1964) from the University of Bristol. After a number of postdoctoral positions in the U.S., Italy (as a Ciba-Geigy fellow), and U.K. (as an ICI fellow), he joined the Division of Chemistry of the National Research Council of Canada in 1968, where he established a group applying computer-simulation techniques to a range of problems in chemical physics. In 1987, he moved to the University of Pennsylvania as Professor of Chemistry. His research interests include the study of structural and dynamical behavior in micelles and model membrane systems, molecular solids, physisorbed monolayers, glasses, and metal–ammonia solutions. He currently holds a John Simon Guggenheim Memorial Fellowship.

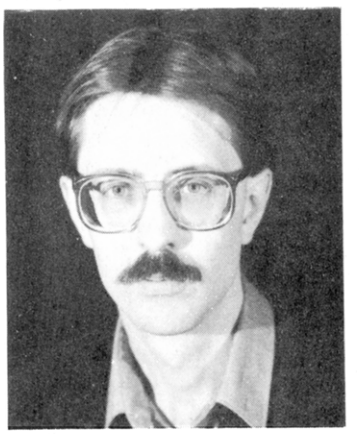

Laurent J. Lewis received a M.Sc. from the University of Ottawa in 1979 and a Ph.D. in Physics from McGill University in 1983. As an NSERC postdoctoral fellow, he spent 2 years at Cornell, where, with Neil Ashcroft, he investigated the dynamic structure of glasses. He returned to Ottawa in 1985, where he joined Mike Klein's computational chemistry group at the National Research Council and became interested in phase transitions and orientational glass formation in molecular solids. In 1986, he moved to the Université de Montréal to become an associate professor. His current research interests include structural phase transitions in ionic atomic and molecular solids, the structure of semiconducting and metallic glasses, and the glass transition.

I. Introduction

The computer-simulation technique called *molecular dynamics* is now routinely applied to study structural and dynamical behavior in solids. Although this technique was originally developed for liquids,[1,2] it was soon realized that phenomena in solids were also prime candidates for study.[3] We refer of course to the fact that the motion of atoms in high-temperature solids is very anharmonic and that such crystals are not perfectly regular solids but invariably contain defects, grain boundaries, etc. Since the implementation of molecular dynamics depends on the "brute-force" solution of the classical dynamical equations on a computer, the advent of larger and faster machines has inevitably led to a proliferation of applications. Thus, phenomena ranging from the glass transition to thermal conduction can now be simulated with the aid of a computer.

At first sight, the use of *classical* Newtonian mechanics to study dynamical behavior in solids may seem somewhat odd. After all, one of the first applications of Planck's *quantum* theory was to explain the specific heat of solids at low temperatures based on the idea

0009-2665/90/0790-0459$09.50/0

that crystal excitations are *quantized* phonons. Moreover, the powerful quantum many-body techniques of solid-state physics that were developed in the late 1950s and early 1960s and reviewed by, for example, Koehler,[4] Barron and Klein,[5] and Horner[6] proved very successful when applied to anharmonic crystals, i.e., the problem of interacting phonons in simple solids. How then can one rationalize the return to a purely classical approach?

The answer to this question lies in the fact that the elegant and formal quantum many-body techniques are not especially well adapted to describe the detailed behavior of complex and highly disordered solids such as mixtures of atomic and molecular components exhibiting simultaneous vibrational motion and rotational diffusion, a situation that arises frequently in nature. Of course, the general phenomena occurring in such crystals are explicable in terms of the basic principles of quantum statistical mechanics, and, indeed, great strides have been made in developing theories of coupled translational and rotational motion.[7,8] It is precisely in keeping track of the details in such complex systems that the computer has come into its own. However, this "simplification" comes about at the expense of using *classical* mechanics.

Molecular-dynamics calculations require as input the intermolecular potentials. Typical model potentials are discussed briefly in section II. Often, such interactions are poorly characterized. Thus, the fact that a molecular-dynamics calculation can yield an essentially exact result for a given system does not imply that the results of a particular molecular-dynamics calculation are necessarily useful: it is vitally important to "calibrate" model potentials against experimental data. Another limitation of the technique, when applied to real systems, is that typically one can only solve the equations of motion for about 10^3 particles. Hence, even with the use of periodic boundary conditions, finite-size effects are difficult to avoid.

As computers become more and more powerful, the limitations mentioned above will no doubt become less important but, for the present, these are real concerns. An impressive body of work on the application of molecular dynamics to the study of dynamical behavior in solids has nevertheless accumulated over the past two decades. This article reviews a selection of work carried out on molecular systems. The reader interested in the finer details of the technique is referred to existing texts (e.g., Ciccotti and Hoover,[9] Allen and Tildesley,[10] and Ciccotti, Frenkel, and McDonald[11]).

We begin section III with a discussion of simple molecular solids. Work on solid nitrogen (N_2), the N_2/Ar alloy, and sulfur hexafluoride (SF_6) is reviewed, along with recent studies on long-chain hydrocarbons. Then, in section IV, we consider ionic molecular crystals in some detail. Here, we present molecular-dynamics results using the Parrinello–Rahman scheme,[12] which allows structural transformations to occur via spontaneous shape changes in the simulation cell. The implementation of this scheme for *molecular* solids was carried out first by Nosé and Klein.[13,14]

An exciting new development has occurred recently whereby molecular dynamics and density-functional theory have been unified into a scheme that extends the range of both techniques. We refer to the work of Car and Parrinello,[15] which has revolutionized electronic structure calculations in disordered materials and inhomogeneous systems. To date, such approaches have mostly been applied to elemental systems,[16-23] but the future will no doubt see further extensions along these lines. This topic clearly deserves a review of its own and hence we will not discuss it further.

II. Formalism

A. Molecular Dynamics

In its simplest form, a molecular-dynamics (MD) simulation involves integration of Newton's equations of motion for a system of N classical particles whose total potential energy U is a function of particle positions. Here, the term "particle" is employed for an atom, an ion, or even a molecule. Iterative integration of the equations of motion yields the trajectories in phase space, i.e., the positions and velocities of all particles as a function of time. Through the ergodic theorem, averages over these trajectories yield ensemble averages.[10]

The equation of motion of particle i, with generalized coordinates $\vec{q}_i$ and mass m_i, can be obtained from Lagrange's equation

$$\frac{\mathrm{d}}{\mathrm{d}t}\left(\frac{\partial L}{\partial \dot{\vec{q}}_i}\right) - \frac{\partial L}{\partial \vec{q}_i} = 0 \tag{1}$$

where L is the Lagrangian:

$$L = L(\{\dot{\vec{q}}^N\},\{\vec{q}^N\}) = K(\{\dot{\vec{q}}^N\}) - U(\{\vec{q}^N\}) \tag{2}$$

The superscript N indicates a function of the coordinates and momenta of *all* N particles in the system. K is the kinetic energy

$$K = \frac{1}{2}\sum_{i=1}^{N} m_i \dot{\vec{q}}_i^{\,2} \tag{3}$$

and depends only on the momenta. Equation 1 thus yields for the force $\vec{F}_i$ on particle i

$$\frac{\mathrm{d}}{\mathrm{d}t}(m_i\dot{\vec{q}}_i) = \frac{\partial L}{\partial \vec{q}_i} = -\frac{\partial U}{\partial \vec{q}_i} \equiv -\nabla_i U = \vec{F}_i = m_i\ddot{\vec{q}}_i \tag{4}$$

Given a model for the potential function $U = U(\{\vec{q}^N\})$, therefore, the trajectory of particle i is determined by solving the second-order differential equation (4). Standard algorithms for performing this integration exist, and we refer the interested reader to the monograph by Allen and Tildesley for an excellent review of the current status of this technique, detailed programming notes, and even listings of code.[10]

It is customary to express the total potential energy U for an atomic system as a sum of n-body interactions, where $n = 1, 2, 3, \ldots, N$:

$$U = \frac{1}{1!}\sum_{i=1}^{N} U_1(\vec{r}_i) + \frac{1}{2!}\sum_{i,j=1}^{N} U_2(\vec{r}_i,\vec{r}_j) + \frac{1}{3!}\sum_{i,j,k=1}^{N} U_3(\vec{r}_i,\vec{r}_j,\vec{r}_k) + \ldots \tag{5}$$

The first term describes the effect of external fields and container walls (surfaces). The second term is due to

pair interactions and depends only on the magnitude of the particle–particle separation:

$$U_2(\vec{r}_i,\vec{r}_j) = U_2(|\vec{r}_i - \vec{r}_j|) \equiv U_2(r_{ij}) \quad (6)$$

Some model pair potentials are discussed in section D. Three-body interactions, though generally important, are not essential to the stability of close-packed systems and can often be neglected in first approximation. In general, little is known about higher order tems, and they are usually ignored. In ultra-high pressure situations, n-body interactions manifest themselves as crystal-field effects which influence the effective size of the atom or molecule in question. This in turn leads to a density-dependent pair potential,[24] which must be taken into account even for insulators.

Systems that have been studied via MD vary greatly in size but typically contain about 10^3 particles. The trajectories of the particles should normally be followed for times substantially longer than the characteristic time of the phenomena one is interested in. Thus, for instance, it is difficult (but not impossible as we shall see) to investigate such phenomena as the glass transition since relaxation processes are known to occur on a very long time scale. Further, the time step must be chosen small enough for accurate integration of the equations of motion, but long enough in order to cover a representative trajectory in phase space. In practice, for a system comprising 10^3 particles, the equations of motion are integrated over 10^4–10^5 time steps of a few femtoseconds, a calculation that may take many hours even on state-of-the-art supercomputers.

In order to mimic an infinite system, i.e., a system with no surfaces, periodic boundary conditions (PBC) are often used. Although such periodically replicated systems are in a sense infinite, various "finite-size effects" may arise. Particularly noteworthy is the impossibility of simulating a phonon with wavelength larger than the size of the MD box. Thus, for instance, very-low-frequency modes, which are relevant to the study of certain phase transitions, may not be accessible in small systems. Nevertheless, it is found that, for systems of practical size, finite-size effects are usually relatively unimportant; that is, a system of 10^3 particles with PBC is adequate to mimic a bulk solid. Recently, simulations have been reported on the crystallization of a system of 10^6 particles;[25] it is claimed that the results are essentially equivalent to those for a system with 10^4 particles.

B. Statistical Ensembles

Integration of the equations of motion for a fixed number of particles N in a constant volume V using the Lagrangian discussed above implies that the total energy E is conserved as a function of time. Thus, the phase–space trajectories generated by virtue of eq 1 sample the microcanonical ensemble, and the time averages taken over such trajectories can be used to characterize the properties of the system in a particular thermodynamic state (N, V, E).

If a system is in equilibrium, its thermodynamic properties can be expressed as time averages of phase–space functions. If we denote an ensemble average by angular brackets, the average total energy is easily evaluated as the sum of average kinetic and potential energies:

$$E = \langle K + U \rangle = \langle K \rangle + \langle U \rangle \quad (7)$$

In the same fashion, we may calculate the average system temperature by using the instantaneous kinetic temperature

$$T = \langle T \rangle = \frac{2}{3Nk_B}\langle K \rangle \quad (8)$$

and the pressure can be obtained from the time average of the virial

$$PV = Nk_BT + \langle W \rangle \quad (9)$$

where

$$W = \frac{1}{3}\sum_{i=1}^{N}\vec{r}_i\cdot\vec{F}_i \quad (10)$$

Methods to sample statistical ensembles other than (N,V,E) also exist. For example, in order to investigate the behavior of a system close to a phase transition, a rigorous control of temperature may be desirable. To accomplish this, the canonical (N,V,T) ensemble may be used. If, in addition, a recrystallization transition is to be modeled, it is then more convenient to work at constant pressure, for instance, in the isothermal–isobaric (N,P,T) ensemble. It is not our purpose to examine in detail the various methods for achieving this end, since this has already been done by Allen and Tildesley,[10] Abraham,[26] and Andersen et al.[27] However, for the benefit of future discussion, we briefly mention those approaches most relevant to the present discussion.

A rigorous method for performing simulations under constant temperature, constant pressure, or a combination of the two was first proposed by Andersen.[28] Andersen's constant-pressure technique, however, only allows one degree of freedom for the MD cell, namely, the *size* (volume). Such an approach is clearly relevant only to the study of isotropic systems, such as liquids and glasses, but not *crystals* where structural transitions involving a change in symmetry can occur. The appropriate theory to handle atomic crystals was developed by Parrinello and Rahman,[12] who allowed the MD cell to also change *shape* by giving total freedom to the cell parameters (i.e., angles and lengths). Generalization of the constant-pressure method to *molecular* solids was achieved by Nosé and Klein.[13,14]

In Andersen's approach, temperature is controlled by subjecting the particles to stochastic collisions. The sudden changes in velocities that result, however, cause the phase–space trajectories to be discontinuous. This problem was addressed by Hoover, Ladd, and Moran[29] and Evans,[30] who proposed an alternative constraint method based on "nonequilibrium" MD. The single most important, and unifying, concept in this field was provided by Nosé.[31,32] In his "extended-system" method, constant temperature is maintained through coupling to an external heat bath. Through the use of an appropriate Lagrangian, the method can be shown to yield *rigorous* canonical ensemble averages; further details can be found in the original articles.

C. Correlation Functions

Molecular-dynamics trajectories can be used to evaluate correlations in both space and time. An example of a spatial correlation function is the "pair

distribution function", $g_N^{(2)}(\vec{r}_1,\vec{r}_2)$, which gives the relative probability of finding a particle at $\vec{r}_2$ given that there is one at $\vec{r}_1$. For a homogeneous system, $g_N^{(2)}$ depends only on the separation between the two particles, $\vec{r} = \vec{r}_1 - \vec{r}_2$, and is referred to as the radial distribution function $g(\vec{r})$. This can be expressed in terms of an ensemble average over a product of single-particle densities

$$\rho(\vec{r}) = \sum_{i=1}^{N} \delta(\vec{r} - \vec{r}_i) \tag{11}$$

as

$$g(\vec{r}) = \frac{V^2}{N^2}\left\langle \sum_{i=1}^{N} \sum_{j\neq i=1}^{N} \delta(\vec{r}_i)\delta(\vec{r}_j - \vec{r}) \right\rangle = \frac{V}{N^2}\left\langle \sum_{i=1}^{N} \sum_{j\neq i=1}^{N} \delta(\vec{r} - \vec{r}_{ij}) \right\rangle \tag{12}$$

where $\vec{r}_{ij} = \vec{r}_i - \vec{r}_j$. In isotropic systems, such as a liquid or a glass, g depends only on $r = |\vec{r}|$. As we shall see, even in a solid, $g(r)$ is still a useful quantity to examine.

The integrated intensity in a scattering experiment is related to the density autocorrelation function in $\vec{Q}$ space

$$S(\vec{Q}) = \frac{1}{N}\langle \rho(\vec{Q})\rho(-\vec{Q}) \rangle \tag{13}$$

where $\rho(\vec{Q})$ is the Fourier transform of the single-particle density $\rho(\vec{r})$:

$$\rho(\vec{Q}) = \sum_{i=1}^{N} e^{-\vec{Q}\cdot\vec{r}_i} \tag{14}$$

$S(\vec{Q})$ is usually referred to as the "static structure factor" and is related to $g(\vec{r})$ by a Fourier transformation; within a multiplicative factor, it is simply the coherent part of the elastic scattering intensity measured in a diffraction experiment, with $\vec{Q}$ the momentum transferred from the incoming particle to the sample.

Time-dependent correlations are naturally of prime interest in the study of dynamical properties of solids. The appropriate generalizations of (12) and (13) are, respectively, the van Hove correlation function[33]

$$G(\vec{r},t) = \frac{1}{N}\left\langle \sum_{i=1}^{N} \sum_{j=1}^{N} \delta[\vec{r} - \vec{r}_i(t) + \vec{r}_j(0)] \right\rangle \tag{15}$$

and its Fourier transform, the "intermediate scattering function"

$$F(\vec{Q},t) = \frac{1}{N}\langle \rho(\vec{Q},t)\rho(-\vec{Q},0) \rangle \tag{16}$$

where $\rho(\vec{Q},t)$ is given by (cf. eq 14)

$$\rho(\vec{Q},t) = \sum_{i=1}^{N} e^{-i\vec{Q}\cdot\vec{r}_i(t)} \tag{17}$$

Thus

$$F(\vec{Q},t) = \frac{1}{N}\sum_{i=1}^{N} \sum_{j=1}^{N} \langle e^{-i\vec{Q}\cdot\vec{r}_i(t)} e^{i\vec{Q}\cdot\vec{r}_j(0)} \rangle \tag{18}$$

The power spectrum, or time Fourier transform, of $F(\vec{Q},t)$

$$S(\vec{Q},\omega) = \frac{1}{2\pi}\int_{-\infty}^{\infty} dt\ e^{i\omega t} F(\vec{Q},t) \tag{19}$$

is called the "dynamic structure factor". Integration of $S(\vec{Q},\omega)$ over the whole energy spectrum leads to an important sum rule relating the static and dynamic structure factors:[34]

$$\int_{-\infty}^{\infty} S(\vec{Q},\omega)\ d\omega = F(\vec{Q},0) = S(\vec{Q}) \tag{20}$$

$S(\vec{Q},\omega)$ is a measure of the coherent (collective) part of the *inelastic* scattering profile. Peaks in $S(\vec{Q},\omega)$ for an ordered solid correspond to phonon-like excitations of the system, and the widths of those peaks are a measure of the phonon lifetimes.

Another time correlation function of interest is the velocity autocorrelation function

$$Z(t) = \tfrac{1}{3}\langle \vec{v}(t)\cdot\vec{v}(0) \rangle \tag{21}$$

time integration of which yields the diffusion constant:

$$D = \int_0^{\infty} Z(t)\ dt \tag{22}$$

This is an example of a Green–Kubo formula, i.e., a formula expressing a macroscopic transport coefficient as the time integral of a microscopic time correlation function. An alternative approach for calculating D involves the Einstein relation

$$D = \lim_{t\to\infty} \frac{w^2(t)}{6t} \tag{23}$$

where $w^2(t)$ is the time-dependent mean-square displacement:

$$w^2(t) = \langle |\vec{r}(t) - \vec{r}(0)|^2 \rangle \tag{24}$$

Thus in a solid, where D is zero, the time integral of $Z(t)$ must vanish, whereas in a liquid, D is finite and the mean-square displacement $w^2(t)$ is expected to increase linearly at large times. For a harmonic solid, the power spectrum of $Z(t)$

$$\tilde{Z}(\omega) = \frac{1}{2\pi}\int_{-\infty}^{\infty} dt\ e^{i\omega t} Z(t) \tag{25}$$

is, to within a normalization factor, equal to the phonon density of states.

D. Models

In the "classical" molecular-dynamics calculations considered here, the rapid motion of the electrons is averaged out (Born–Oppenheimer approximation) and the microscopic state of a system is described in terms of nuclear positions and velocities. As discussed in section A, a system's dynamics is driven by the forces $\vec{F}_i = -\vec{\nabla}_i U$. The bulk (≈95%) of computer time in an MD experiment is devoted to the evaluation of these forces (the so-called "force loop" over particles).[10] It is therefore pragmatic, for many applications, to "sacrifice" the higher order many-body interactions in eq 5 in favor of speed of execution. Accordingly, we restrict our subsequent discussion to effective pair potentials parametrized to experimental data. (We stress that many-body interactions are necessary for *quantitative* modeling of condensed-state systems.)

The most popular effective pair potential continues to be the Lennard-Jones form

$$U_{LJ}(r) = 4\epsilon\left[\left(\frac{\sigma}{r}\right)^{12} - \left(\frac{\sigma}{r}\right)^{6}\right] \tag{26}$$

where σ is the atomic diameter and ϵ is the depth of the

well. This model, of course, is not precise *even* for the interactions between rare-gas atoms but is nevertheless extremely useful as a first approximation. Another perennial favorite is the Buckingham potential[35]

$$U_B(r) = Ae^{-ar} - B/r^6 \tag{27}$$

Interactions between unlike atoms in polyatomic systems, if not available directly, can be approximated by using "combining" (or "mixing") rules, such as Lorentz-Berthelot. For the Buckingham potential, we use

$$\begin{aligned} A_{\alpha\beta} &= (A_{\alpha\alpha}A_{\beta\beta})^{1/2} \\ a_{\alpha\beta} &= \tfrac{1}{2}(a_{\alpha\alpha} + a_{\beta\beta}) \\ B_{\alpha\beta} &= (B_{\alpha\alpha}B_{\beta\beta})^{1/2} \end{aligned} \tag{28}$$

Such rules are, of course, totally empirical. More precise models for pair potentials have been discussed by Maitland et al.[36] and more recently by Price and Stone.[37]

For ion–ion interactions, the short-range pair potentials discussed above must be augmented by long-range Coulomb interactions

$$U_C(r_{ij}) = \frac{z_i z_j}{4\pi\epsilon_0 r_{ij}} \tag{29}$$

where z_i is the charge on atom i and ϵ_0 is the permittivity of free space. Coulomb forces, because of their long interaction range, are difficult to evaluate. Accordingly, for solids, special techniques such as the Ewald summation must be used.[10]

Finally, in ionic systems, induced dipole–induced dipole interactions may also be important. Since this interaction is not pairwise additive, it is more difficult to deal with. The famous "shell model" of Cochran, Dick, and Overhauser provides a zeroth-order solution to this problem.[38] For molecular systems, pragmatic considerations such as limitations of computer time often dictate neglect of such terms (however, see Sprik and Klein).[39]

Real (i.e., *flexible*) molecules require special treatment for two reasons. First, classical potentials such as those described above cannot be expected to give a proper description of intramolecular (valence) interactions. Second, internal vibrations are generally of high frequency (though of low amplitude), and hence quantum at room temperature. It is troublesome to treat this high-frequency motion concurrently with center-of-mass translations. It is therefore customary to regard small molecules as rigid entities with fixed bond lengths and/or angles. Long-chain molecules are treated as having flexible backbones,[40] but special constraint techniques are also employed.[41]

For molecules, the charge distribution is usually represented by partial (static) charges, chosen such as to reproduce as closely as possible the known multipole moments of the real distribution. Note that atomic sites and charges do not necessarily coincide. Models of this type can give a surprisingly good description of the moments of the charge distribution of selected molecules, such as an in-crystal CN^- ion.[42]

Intermolecular interactions are usually dealt with using the site–site approximation, whereby sites (i.e., the atoms and charges referred to above) on distinct molecules interact pairwise additively. Interactions between sites within the same molecule are often neglected by virtue of the rigid-molecule approximation, but for flexible molecules, intramolecular site–site interactions are often included.[40] Finally, we mention that nonspherical atom–atom potentials have been invoked recently with great success.[37]

III. Molecular Crystals

When a molecular liquid is cooled, translational and orientational degrees of freedom do not necessarily freeze at the same temperature. Most often, the system condenses into a phase where the molecular centers of mass order on a crystalline lattice, but not the orientations. In this so-called "plastic-crystal" or "rotator" phase, molecules continue to udergo rotational diffusion. The complementary situation occurs for oblate- or prolate-shaped molecules forming a "liquid crystal"; here, orientations are fixed, but centers of mass diffuse.

Ordered molecular crystals that exhibit small-amplitude vibrations are well treated by using lattice dynamics in the harmonic approximation.[43,44] The outstanding issues relate to questions of potentials[45] as well as the nature of anharmonic effects, which continue to attract attention.

Molecular systems that are orientationally disordered or that exhibit strong anharmonicity are not readily amenable to treatments via analytic theories. Progress in the understanding of collective excitations in disordered molecular solids has therefore been slow (see, however, the work by Michel and Rowe[7,46] and by de Raedt and Michel[47]). Experimentally, librational modes are difficult to observe in rotator phases because the motion is often overdamped. On the other hand, acoustic (i.e., low frequency—or sound) modes can be resolved for small momentum transfer via Brillouin and neutron scattering. As selected examples of the progress made to date in understanding molecular crystals, we review results on the simplest nonionic molecular solids, namely, N_2, N_2:Ar alloys, and SF_6.

A. Solid Nitrogen

On cooling from the melt under its own vapor pressure, liquid N_2 solidifies at $T \approx 63$ K into an hexagonal lattice with nearly ideal c/a ratio—the β phase. NMR experiments indicate that N_2 molecules reorient in a time much less than $\approx 10^{-7}$ s.[48] On further cooling, the β phase transforms at $T \approx 35$ K into the α phase, which is a cubic $Pa3$ structure. The β phase also forms on crystallizing the high-pressure liquid. At low temperature and pressures in excess of ≈ 5 kbar, solid α-N_2 transforms to γ-N_2, a tetragonal system with two molecules per unit cell. At still higher pressures, additional ordered and disordered phases exist which are presently the subject of active research.[14,49,50]

Early self-consistent phonon calculations for α-N_2 by Raich and co-workers[51,52] have demonstrated that agreement with experiment could be obtained with a simple atom–atom 6–12 potential. However, this model was unable to predict the $\alpha \rightarrow \gamma$ transition:[53,54] the potential just does not yield the correct anisotropic forces.[55] Raich and Gillis later performed a careful determination of the intermolecular potential and investigated the dynamics of both α and γ ordered phases.[56] The new model assumed pairwise additivity,

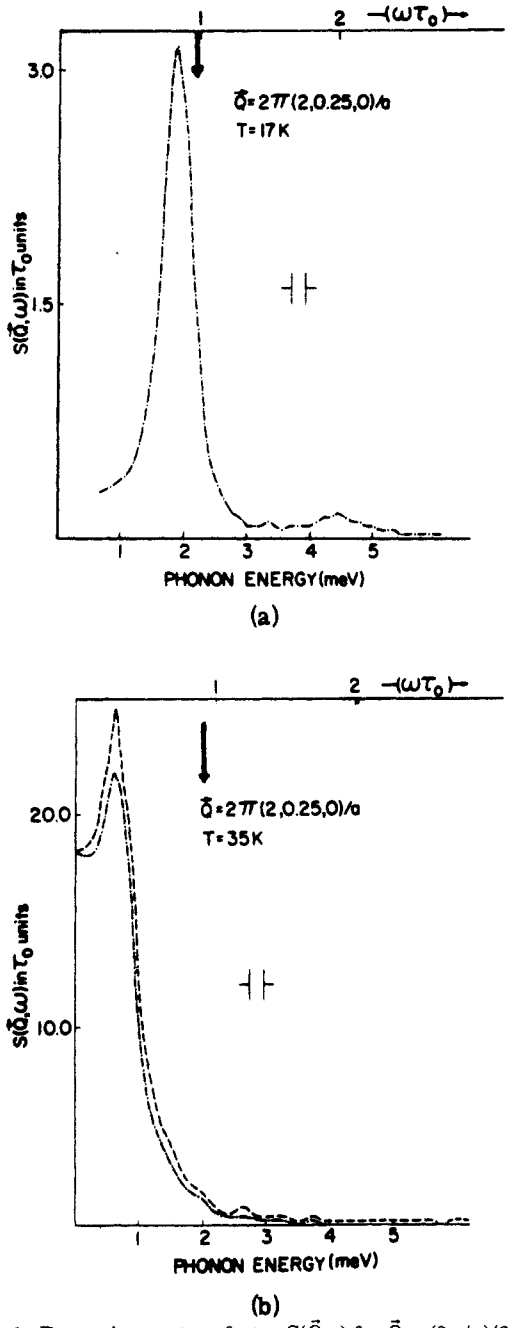

Figure 1. Dynamic structure factor $S(\vec{Q},\omega)$ for $\vec{Q} = (2\pi/a)(2,1/4,0)$ in solid α-N_2 at (a) 17 K and (b) 35 K. Arrows indicate the quasiharmonic peak positions; in (b), the dashed line indicates the effect of incorporating the Schofield correction to account for detailed balance. Reprinted from ref 57; copyright 1975 American Institute of Physics.

i.e., neglected the influence of three-body and higher order forces, which likely accounts for a substantial ($\sim$10%) portion of the sublimation energy (recall section II).

Molecular-dynamics simulations of solid N_2 were performed in the α phase by Weis and Klein[57] and in the β phase by Klein and Weis[58] and Klein, Lévesque, and Weis.[59] In the former two studies, a simple Lennard-Jones 6–12 potential was employed, while in the latter, the more realistic Raich–Gillis model[56] was utilized. We first briefly discuss the results for the orientationally ordered α phase.

Figure 1 shows one example of the calculated dynamic structure factor $S(\vec{Q},\omega)$ at two temperatures for the transverse acoustic (TA) phonon with wavevector

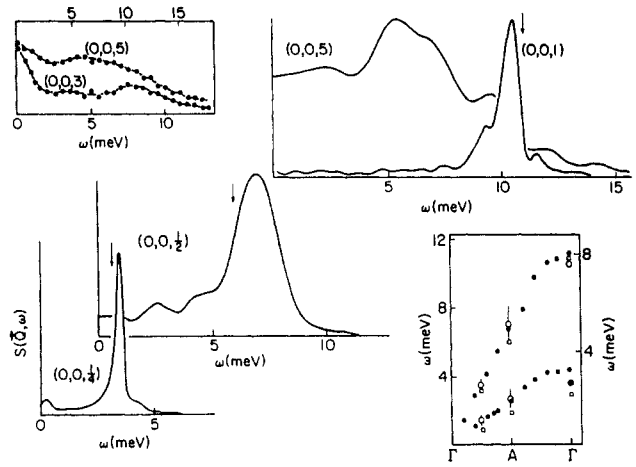

Figure 2. Dynamic structure factor $S(\vec{Q},\omega)$ for longitudinal phonons propagating along the c axis in solid β-N_2. Wavevectors are labeled by $(0,0,\xi) = a\vec{Q}/2\pi$. Arrows indicate the peak positions obtained in an earlier calculation using a simpler potential (see text). The inset in the upper left shows the experimental data of Dolling[60] (lines are a guide to the eye; see text for details); the inset in the lower right compares experimental (closed symbols) and theoretical (open symbols) phonon dispersion curves for both longitudinal and transverse modes. Reprinted from ref 59; copyright 1981 American Institute of Physics.

$\vec{Q} = (2\pi/a)(2,1/4,0)$, i.e., one-quarter of the way to the zone boundary. Most remarkable is the considerable negative shift in frequency that takes place as temperature is increased. The appearance of a large quasielastic (central) peak in the MD spectrum signals the presence of rotational diffusion. The corresponding longitudinal phonon (not shown) exhibits no such anharmonic shift and no quasielastic scattering either. Overall agreement with experimental data on lattice modes was good except for high-frequency modes, which are off by about 20%, owing to the inadequacy of the Lennard-Jones potential as well as the absence of electrostatic quadrupole–quadrupole terms. A comparison with the results of quasiharmonic lattice dynamics (arrows in Figure 1), using essentially the same potentials, clearly demonstrates the importance of anharmonic terms in solid α-N_2.[51,52,54]

In an early study of β-N_2,[58] Klein and Weis employed, as mentioned above, a simple 6–12 potential fitted to the liquid-state properties. Even though many of the experimental observations on β-N_2 could be understood on the basis of this model, quantitative agreement was often lacking. For instance, the ratio c_l/c_t of longitudinal to transverse sound speeds for waves propagating along the c axis was found to be $\approx$50% too large. Further, while neutron scattering showed clear evidence not only for rotational diffusion but also for librational motion, this evidence was found to be less prominent in the MD experiment. Another series of simulations were consequently carried out by Klein, Lévesque, and Weis,[59] this time using the more realistic Raich–Gillis potential discussed above.[56] The system studied consisted of 288 molecules disposed on a hexagonal lattice of volume $V = 26.1$ cm^3/mol at $T = 47$ K. The main difference from earlier work was the inclusion of the electrostatic quadrupole–quadrupole interaction between molecules, which was incorporated by using charged sites.

Figure 2 shows the dynamic structure factor $S(\vec{Q},\omega)$ for selected longitudinal phonons propagating along the

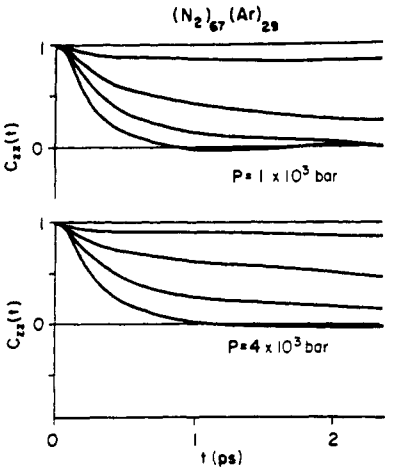

Figure 3. Temperature dependence of the single-molecule reorientational autocorrelation function (eq 30) in computer-simulated $(N_2)_{67}(Ar)_{29}$ at two different pressures. Curves correspond, from bottom to top, to T = 60, 40, 20, and 10 K, respectively; note the nondecaying components at low temperatures. Reprinted from ref 64; copyright 1985 National Research Council of Canada.

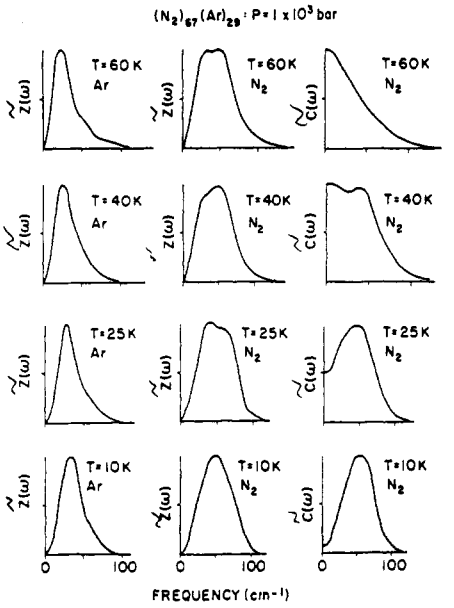

Figure 4. Power spectra for translational, $\tilde{Z}(\omega)$, and librational, $\tilde{C}(\omega)$, motion in $(N_2)_{67}(Ar)_{29}$ at P = 1 kbar and four different temperatures. Reprinted from ref 64; copyright 1985 National Research Council of Canada.

c axis. Indicated by arrows for comparison are the peak positions determined from the earlier calculations with the simpler 6–12 pair potential. The translational phonons are well defined, with the broadest response at the A point of the Brillouin zone. On increasing momentum transfer, the phonon peaks disappear [cf. curve labeled (0,0,5)] and are replaced by an ill-defined maximum around 6 meV superimposed on a broader central peak which is due to rotational diffusion. The peak at 6 meV was absent in the earlier calculation. The inset in the upper left corner shows two experimental neutron profiles measured at V = 28.0 cm³/mol and T = 36 K.[60] The upper energy scale includes a correction to allow for the differences in state conditions between experiment and MD. The overall agreement is quite good. The inset in the lower right corner of Figure 2 compares the calculated and measured dispersion curves for longitudinal and transverse phonons propagating along the c axis, again taking into account a correction for the different state conditions. Shown as squares are the results of the earlier simulation. Clearly, the second model represents a considerable improvement over the first one and, in particular, the ratio of sound velocities c_l/c_t is now found to agree much better with Brillouin scattering data.[61]

B. $(N_2)_{67}(Ar)_{29}$ Alloy

On dilution of the N_2 lattice with more than ~22% but less than ~42% Ar atoms, the crystal is found to bypass the $\beta \rightarrow \alpha$ transition mentioned above and remain hexagonal down to the lowest temperatures. Inelastic neutron scattering experiments[62] show that at high temperatures, the system is in a state of rotational diffusion (rotator phase), while at lower temperatures, there is a gradual freezing out of the molecular orientations into a state that lacks long-range orientational order, though there is evidence that short-range order is present. Such a state is called an "orientational glass", by analogy with topological, or "translational", glass. N_2–Ar solid solutions can be regarded as classical analogues of orthohydrogen–parahydrogen mixtures,[63] and as such are more readily suited to study by classical simulation techniques.

Such an MD study of the $(N_2)_{67}(Ar)_{29}$ mixture was carried out by Nosé and Klein.[64] The atoms were chosen for simplicity to interact via appropriate Lennard-Jones 6–12 potentials, plus the electrostatic quadrupole–quadrupole term between N_2 molecules. Figure 3 shows the orientational autocorrelation function $C_{zz}(t)$ of N_2 molecules, defined as

$$C_{zz}(t) = \langle [3z^2(t) - 1][3z^2(0) - 1] \rangle \qquad (30)$$

where z is the projection of the N–N bond on the crystal c axis. Clearly, there is a dramatic slowing down of molecular reorientations as temperature is reduced from 60 to 10 K. Just as with structural glasses,[65] there appears a nondecaying component in $C_{zz}(t)$ and, on the time scale of the simulation, the system is in a state of orientational structural arrest, in qualitative agreement with neutron measurements.[62]

The gross features of the dynamics of this molecular system can be probed by the translational and angular velocity autocorrelation functions, the power spectra of which yield the phonon and libron densities of states, respectively (cf. eq 25). These are shown in Figure 4 at four different temperatures. The power spectra $\tilde{Z}(\omega)$ for translational motion are much narrower for Ar atoms than they are for N_2 molecules. On the other hand, the spectrum for orientational motion, $\tilde{C}(\omega)$, evolves from a broad featureless wing at high temperature to a single-peak spectrum at low temperature. This is likely the signature of collective librational modes, as no oscillations are apparent in the single-molecule autocorrelation function $C_{zz}(t)$ at T = 10 K (cf. Figure 3). Note that the high-frequency part of $\tilde{Z}(\omega)$ for N_2 is nothing more than the corresponding part of $\tilde{C}(\omega)$, which indicates that there is likely a coupling between the translational and the rotational degrees of freedom of the N_2 molecules. We will return to the investigation of such questions in the course of our discussion of the mixed cyanides. Recent work on the N_2/Ar alloy has been presented by Klee, Carmesin, and Knorr.[66]

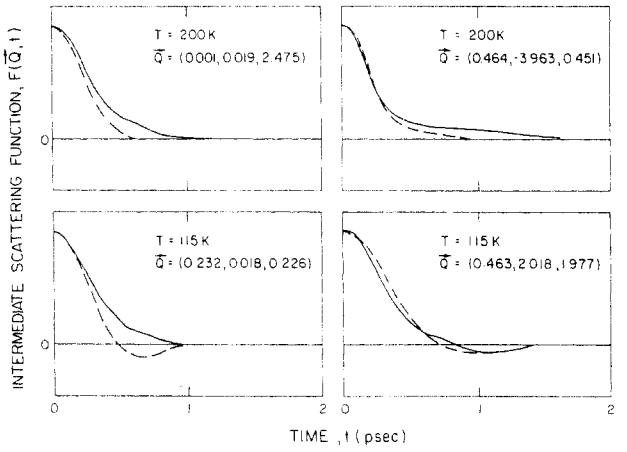

Figure 5. Intermediate scattering function $F(\vec{Q},t)$ versus time for selected phonons at two different temperatures in sulfur hexafluoride ($\vec{Q}$ is in units of $2\pi/a$). The full line shows the total $F(\vec{Q},t)$, while the dashed line shows the corresponding center-of-mass function. Reprinted from ref 72; copyright 1986 Taylor & Francis Inc.

C. Sulfur Hexafluoride

The high-temperature phase of sulfur hexafluoride is bcc (point group O_h) and extends from the sublimation point at 223 K down to about 96 K. The molecules undergo reorientational motion, as evidenced by NMR measurements.[67] The orientational distribution function $P(\Omega)$ for the S–F arms of the octahedral SF_6 molecule is found to possess maxima along the cube axes, though the function has significant value at angles as much as 20° away from these directions:[68] perfect alignment along the cube axes is prevented by steric hindrance. Thus, rotational motion is not free, but correlations exist betwen neighboring molecules. Also, calculations of the intermolecular potential show the force between nearest-neighbor molecules to be attractive when they align parallel to the cube axes, while the force between *second* nearest neigbors is repulsive in the same geometry.[69,70] The competition between these two contributions means that the molecules do not feel a well-defined orientational potential. This effect was referred to as "orientational frustration" by Dove and Pawley,[69,70] who suggested that it may well be fundamental to the existence of orientational disorder in this system. At high temperatures, a crystal lattice of high symmetry is produced, because the frustration is dynamically averaged. At 96 K, the system undergoes a phase transition to a monoclinic structure.[71]

The experimentally determined picture of SF_6 has been augmented by an extensive series of MD simulations[69–73] carried out on a distributed array processor (DAP) with a sample consisting of 4096 molecules (one for each processor). The model consisted of rigid SF_6 molecules with F atoms interacting via nearest-neighbor Lennard-Jones potentials. The MD calculations confirmed the observed orientational distribution function, and no evidence was found for the existence of well-defined collective librational modes.

Figure 5 shows typical examples of the intermediate scattering function (eq 16) calculated from the phase-space trajectories of the MD experiment. $F(\vec{Q},t)$ is seen to decay rapidly to noise level before even the first node in the function's oscillation is reached. Hence, no well-defined collective excitation exist; the normal modes are overdamped, as indeed observed experimentally. Note in Figure 5 the similarity between the *total* scattering function and its center-of-mass counterpart; this suggests strong coupling between translational and rotational degrees of freedom in this system. Thus, purely librational modes cannot propagate in this orientationally frustrated crystal.

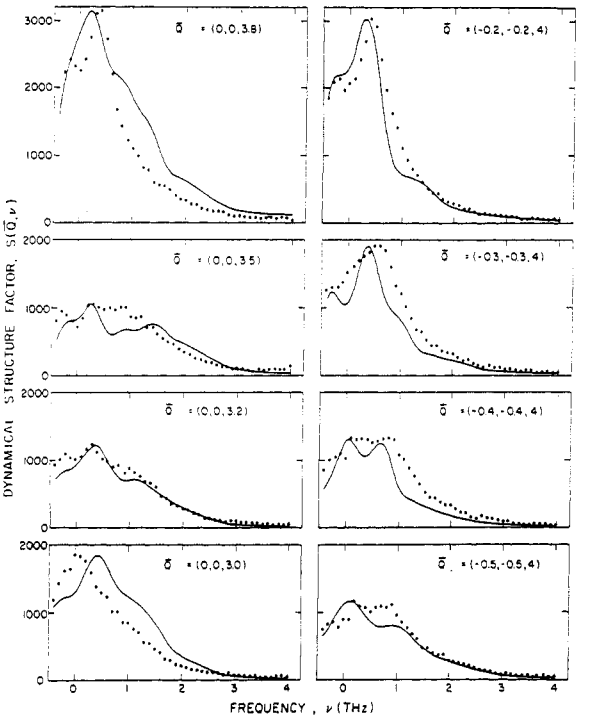

Figure 6. Comparison between observed and MD-calculated dynamic structure factors for momentum transfers along the [100] and [110] symmetry directions near the $(2\pi/a)(0,0,4)$ reciprocal lattice point in sulfur hexafluoride. Dots show the experimental data after subtraction of the background; full lines shows the MD data after convolution with the experimental resolution function. Reprinted from ref 72; copyright 1986 Taylor & Francis.

In contrast to the case discussed above, the scattering function for center-of-mass motion *for the smallest available wavevector* in the computer-simulated system exhibits well-defined long-lived excitations. Thus, close to the Brillouin zone center, acoustic modes are well defined, but their lifetime decreases as one gets away from the zone center. One also sees from this figure that increasing temperature results in increased damping.

The calculated and measured dynamic structure factors are compared in Figure 6 for eight values of wavevector along the [001] and [110] directions. Overall agreement between the two is clearly extremely good, though there are small discrepancies in both peak positions and intensities. These small differences may be due in part to the oversimplified resolution function used to deconvolute the experimental data, to truncation errors in the Fourier transformation of the MD data, or most likely to the simple nature of the intermolecular potential.

D. *n*-Alkanes

The complexity of the phase diagrams exhibited by long-chain molecules near their respective melting points has become apparent only in recent years. Stable solid phases have been identified that contain both conformational and orientational disorder.[74,75] Moreo-

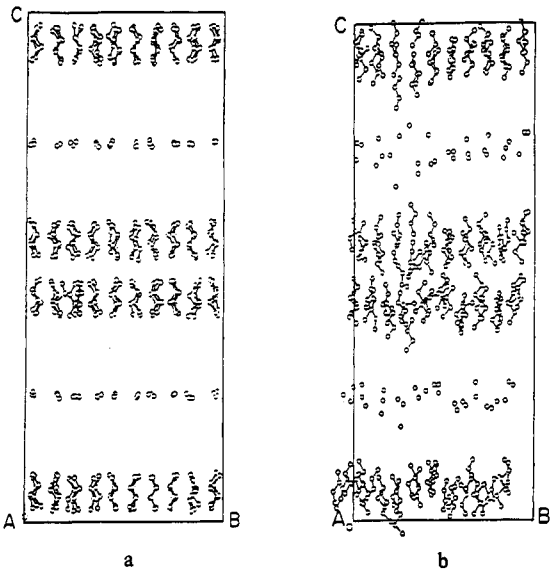

Figure 7. Instantaneous configurations of the bilayer *n*-alkane $C_{23}H_{48}$(tricosane) viewed down the *a* axis (a) in the crystalline orthorhombic phase at 38 °C and (b) in the pseudohexagonal phase at 42 °C. For clarity, no H atoms and only the terminal plus the central C atoms are shown. The disorder at the interface is dominated by longitudinal diffusion of the chains, as is clearly exhibited by the enhanced fluctuations in the position of the central C atoms in case (b). Reprinted from ref 78; copyright 1987 American Institute of Physics.

ver, the number and character of these phases vary with the molecular chain length.[75] In *n*-alkanes, experiments based on diffraction[76] and spectroscopic[74] techniques as well as calorimetric and NMR studies[77] have established that when the crystalline phase transforms to the pseudohexagonal rotator phase, the longitudinal diffusive motion of the chains increases dramatically and a significant concentration of conformational defects is generated, predominantly in the vicinity of the interface between layers of alkanes (cf. Figure 7a).

In order to further characterize the nature of the bilayer interface, a molecular-dynamics study of the structure and dynamics of the *n*-alkane $C_{23}H_{48}$ (tricosane) in both the crystalline and pseudohexagonal rotator phases close to the phase transition temperature of 40 °C was carried out by Ryckaert, Klein, and McDonald.[78,79] In the crystalline phase, *n*-alkane chains adopt their all-trans most elongated conformation and pack in a lamellar bilayer structure. Within each layer, the molecular longitudinal axes are mutually parallel, and the planar zigzag chains have two possible orientations. Thus, there are four molecules per unit cell. The experimental lattice constants for crystalline tricosane are a = 7.47 Å, b = 4.98 Å, and c = 62.40 Å.[80] The transformation from the crystalline phase to the pseudohexagonal rotator phase (sometimes referred to as face-centered orthorhombic) takes place around 40 °C, where the lattice parameters take the values a = 8.00 Å, b = 4.85 Å, and c = 63.22 Å.[75,76]

The MD calculations of Ryckaert, Klein, and McDonald have been carried out on periodically replicated bilayer systems arranged as 3 × 5 unit cells in the (a,b) plane. The sample contained only one unit cell in the c direction, so that the total system consisted of 60 chains (4260 atoms). Because of the boundary conditions, there are two distinct interfaces. The calculation made use of a microscopic model based on flexible (semirigid) chains and atom–atom intermolecular potentials, as well as intramolecular potentials consisting of bending and torsional terms, plus methylene–methylene group interactions.[81] The equations of motion were integrated by standard methods.[82] Full details can be found in the original papers.[78,79]

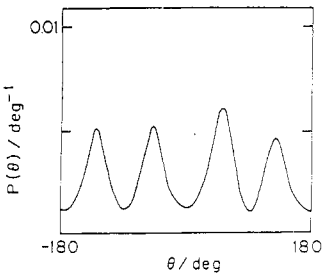

Figure 8. Orientational probability distribution of the chains, with respect to the crystal *a* axis, in the rotator phase. Reprinted from ref 79; copyright 1989 Taylor & Francis Inc.

Figure 7a shows a typical instantaneous configuration of the system in the crystalline phase (at 38 °C) viewed down the crystal *a* axis. The system is very stable in this phase, the bilayer interface is very well defined, and, even though the temperature is very close to the melting point, only modest longitudinal displacements of the chains can be observed. An instantaneous configuration of the bilayer rotator phase, now, is shown in Figure 7b. Although the temperature is only 4 °C higher than in the crystalline phase (and the cross-sectional area per chain has been increased by a mere 6% to account for the different crystal structures), it is immediately evident that considerable disorder is now present. The system is nevertheless stable, as can be appreciated by the ease at which temperature could be controlled and by the fact that the calculated internal stress-tensor components were all small (i.e., less than about 1 kbar).

The mechanism of rotational disorder in this system is of interest. In the crystalline phase, one instance of a rotational defect was observed, which appeared and subsequently disappeared over a period of about 200 time steps, but the system was otherwise found to remain fully ordered. This contrasts strongly with the behavior found in the rotator phase, where the four-site orientational distribution—corresponding to the four possible orientations of each chain, located at ±35° and ±135° with respect to the crystal *b* axis—appears to be quite stable (Figure 8). The mean residence time between jumps was estimated to be 13 ps, which compares favorably with values based on neutron scattering measurements.[83] Even though both simulations were carried out at essentially the same temperature, the much larger dispersion in the positions of the chain centers of mass in Figure 7b compared with that in Figure 7a indicates the presence of enhanced longitudinal chain displacements in the rotator phase. The root-mean-square chain displacement along the c axis is calculated to be about 2 Å, which compares well with the value 1.7 Å estimated from small-angle X-ray diffraction data.[76]

Figure 7b also reveals the presence of intramolecular defects in the rotator phase. The presence of a gauche defect, two of which are clearly visible, causes a chain to shorten by about 1.1 Å. On average, about 10% of the chain ends are found to have gauche defects,[79] a concentration which implies that the average chain length is shortened by 2 × 0.10 × 1.1 Å = 0.22 Å. The

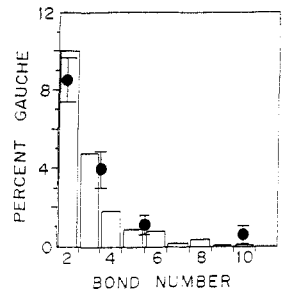

Figure 9. Distribution of gauche defects along the chain backbone. The filled circles are experimental data for *n*-heneicosane, $C_{21}H_{44}$,[74] while the histogram is the computed distribution. Reprinted from ref 79; copyright 1989 Taylor & Francis Inc.

actual mean end-to-end chain length in the rotator phase was found to be shortened by about 0.30 Å, i.e., a value much too large to be attributed solely to the presence of gauche defects. It is therefore very likely that chains are shortened predominantly via torsional motion.

The calculated percentage of gauche defects at various positions along the *n*-alkane chain backbone is compared in Figure 9 with that measured in the closely related system $C_{21}H_{44}$.[74] Both calculation and experiment suggest an exponential growth of defects toward the chain ends; overall, the agreement with experiment is surprisingly good (see also ref 77).

It seems reasonable to assume that the bilayer interface is the most hospitable place for the birth of intramolecular defects. On one occasion, however, the spontaneous formation of a defect in the middle of a chain was observed, which then proceeded to migrate toward the chain end. This suggests that the birth and death of intramolecular defects might profitably be modeled in terms of soliton dynamics.

IV. Ionic Molecular Solids

As with ordinary molecular solids, orientational disorder is a common feature of ionic molecular crystals. Indeed, there may even be more than one disordered phase. Ionic crystals are good examples of nearly classical—but also strongly anharmonic—systems and are therefore well suited to study by MD. In the remainder of this section, we review the studies carried out on a few selected solids, each of which exemplifies certain novel structural and dynamical features.

A. Ammonium Bromide

In its high-temperature α phase, NH_4Br has the NaCl-type structure, with the NH_4^+ tetrahedral ions undergoing relatively rapid reorientations. Little is known experimentally about the nature of the disorder. In the corresponding phase of ND_4I, neutron diffraction experiments show that the arms of the tetrahedron lie preferentially along [100] directions.[84] On cooling at atmospheric pressure, there is a transition at 411 K to a CsCl-like eightfold-coordinated β phase. Neutron experiments of the corresponding phase in ND_4Br show that there is a flipping between orientations in which the N–D bond vectors lie along the [111] direction. There is a second transition to the so-called γ phase at 235 K; here, the tetrahedra are ordered in an antiferro arrangement, with a weak tetragonal distortion.[85] Finally, at still lower temperatures, in the δ phase, the

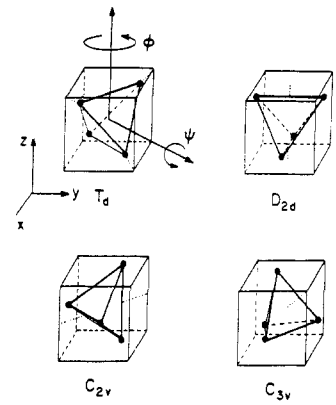

Figure 10. The four ideal orientations of a tetrahedron in a cubic field. Reprinted from ref 86; copyright 1983 American Institute of Physics.

structure is again cubic, but the ions are ferro aligned.

The four "ideal" configurations of the NH_4^+ molecule, i.e., those configurations most relevant to the reorientational motion of a tetrahedron in a cubic field, are displayed in Figure 10 and labeled T_d, D_{2d}, C_{2v}, and C_{3v}. Neutron measurements suggest that the α phase (of ND_4I) is mostly C_{3v}, while the β phase is mostly T_d.

As in many similar problems, it is convenient to expand $P(\Omega)$, the orientational distribution function, in terms of symmetry-adapted functions. Here, it is appropriate to use the tetrahedral rotor functions of order l, where $l = 1, 2, \ldots$. For each value of l, there are $(2l + 1)$ functions, and the first nonvanishing ones for a tetrahedron are those for $l = 3$, labeled $M_\mu(\hat{u})$, where $\mu = 1, \ldots, 7$ and $\hat{u} \equiv (x,y,z)$ is a unit vector along the N–H bond. The expectation values of these functions vanish in the disordered phase, so that the fluctuations $\langle M_\mu^2 \rangle$ serve as order parameters. Because the crystal has cubic symmetry, there are only three independent functions, with degeneracies 1:3:3, respectively, namely

$$M_1 = \frac{3\sqrt{3}}{4}\sum_{i=1}^{4} x_i y_i z_i$$

$$M_2 = \frac{3\sqrt{5}}{40}\sum_{i=1}^{4} x_i(5x_i^2 - 3) \qquad (31)$$

$$M_5 = \frac{3\sqrt{3}}{8}\sum_{i=1}^{4} x_i(y_i^2 - z_i^2)$$

corresponding respectively to T_d, C_{3v}, and D_{2d} symmetries. The sums are over all four N–H branches of the tetrahedron. Time-dependent correlations of the quantities M_μ will be used below to gain insight on the dynamical nature of the orientational disorder.

A MD study of the α and β phases of NH_4Br was carried out by Klein, McDonald, and Ozaki.[86] The molecular ions were treated as unpolarizable and rigid, with a N–H bond length of 1.03 Å. Short-range interactions were modeled by appropriate Buckingham-type potentials taken from the work of Tosi and Fumi.[35] The charge distribution of NH_4^+ was determined on the basis of an ab initio calculation of the octupole moment, and the corresponding interactions were handled by the Ewald method.[10] Rather small systems, consisting of $N = 32$ and 64 ions of each species, were used to simulate the α and β phases, respectively.

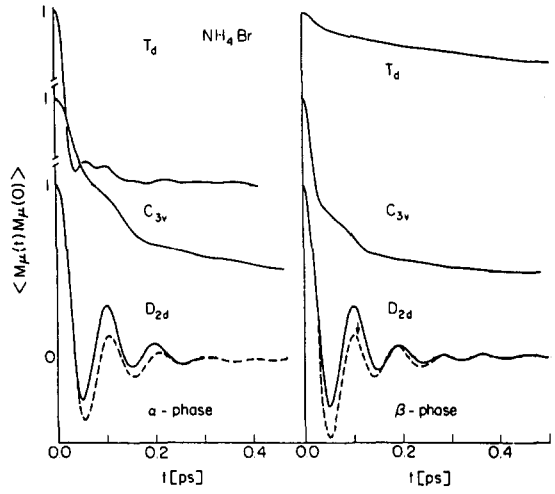

Figure 11. Single-ion order parameter autocorrelation function (full curve) and velocity autocorrelation function of the protons (dashed curve) in the disordered α and β phases of NH_4Br. The arrow indicates the experimental value for the period of oscillation of the NH_4^+ ion. Reprinted from ref 86; copyright 1983 American Institute of Physics.

A question of considerable interest concerns the persistence of orientational order of a given type. This is available from MD through a study of the decay of the corresponding order parameters. Thus we show in Figure 11 the time-dependent correlation functions $\langle M_\mu(t)M_\mu(0)\rangle$ for $\mu = 1$, 2, and 5. It is clear that there is no strongly persistent order of any character in the α phase, though C_{3v} is the longest lived. On passing to the β phase, however, the C_{3v} and D_{2d} functions are essentially unaltered, but the lifetime of the T_d correlation function lengthens markedly. The latter decays exponentially, with a relaxation time of about 3 ps, in qualitative agreement with experiment.

The oscillations of the D_{2d} function are strongly suggestive of librational motion of the tetrahedra. To ascertain whether or not this is so, Figure 11 also shows the velocity–velocity correlation function for the protons, and indeed, both correlate strongly. The frequency of oscillation is in good agreement with spectroscopic data (indicated by the arrow in Figure 11).

Coherent inelastic scattering measurements of the β phase suggest that the rotational motion of the NH_4^+ ions is very slow and that it couples to the translational motion, as evidenced primarily by the appearance of a central peak in the energy spectrum of scattered neutrons.[87] Translation–rotation coupling can however be seen in another way. The transition from the β to the γ phase involves the appearance of two sublattices, i.e., the freezing-out in the β phase of a zone-boundary phonon of appropriate symmetry. The phonon in question is the Brillouin-zone M-point TA_2 mode, whose pattern of displacements is shown in the inset to Figure 12. Since the NH_4^+ ions are at rest here, one expects a splitting of the second-neighbor Br–Br separation. This is clearly visible in the results for $g_{Br-Br}(r)$, plotted in Figure 12. By contrast, $g_{N-N}(r)$ shows no such distortion. These results provide strong evidence of a translation–rotation interaction which could act as a precursor to the M-point instability and ultimately lead to the $\beta \rightarrow \gamma$ transition. The effect can also be studied dynamically by examining the intermediate scattering function associated with the M-point phonon, $\vec{Q} = (2\pi/a)(1/2,1/2,1)$. It was found that the function $F(\vec{Q},t)$

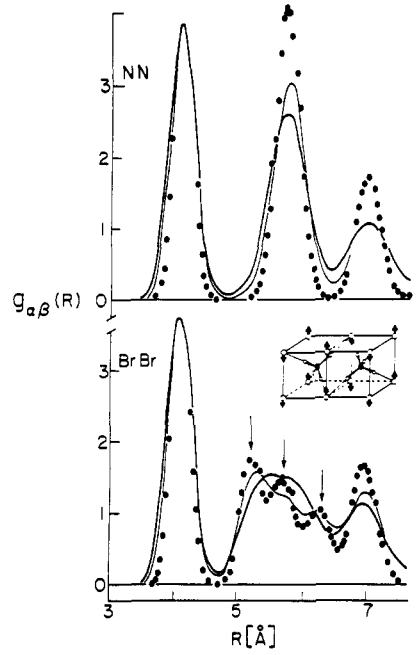

Figure 12. Partial N–N and Br–Br radial distribution functions for the β phase of NH_4Br. Bold and thin curves correspond to $T = 410$ and 344 K, respectively, while dots are for $T = 235$ K. The inset shows the halide ion displacement pattern for the M-point TA_2 phonon. Reprinted from ref 86; copyright 1983 American Institute of Physics.

for the M-point phonon clearly exhibits a long-time tail, corresponding to a strong central peak in the dynamic structure factor, which, in turn, suggests that the molecular ions are in a state of quasistatic orientational order. Thus, MD studies fully confirm the interpretation of the neutron data.[87]

B. Lithium Sulfate

The high-temperature (α) phase of Li_2SO_4 is an example of a plastic crystal that also behaves as a solid electrolyte. As in other rotator phase solids, the presence of orientational disorder restricts the amount of structural information that can be extracted from diffraction data. The latter nevertheless reveal that SO_4^{2-} ions lie on a fcc lattice, the Li^+ ions occupying the sites of an interpenetrating simple cubic lattice; thus, each SO_4^{2-} ion is surrounded by eight Li^+ ions.[88] Also, the best fit to the Bragg intensities is obtained by assuming the SO_4^{2-} angular distribution function to be isotropic. For such a complex system, MD studies offer the prospect of characterizing the microscopic behavior in greater detail than can be provided by experiment.

Such calculations were carried out by Impey, Klein, and McDonald on systems of either 96 or 324 ions interacting via appropriate Buckingham exp-6 potentials.[89,90] Periodic boundary conditions were again used to simulate an infinite crystal. The charge distribution of the SO_4^{2-} ion was represented by a five-point model, the charge on the oxygen atom being either $Q_O = -0.5$ e (model I) or −0.8 e (model II); the latter is in better agreement with ab initio calculations of the sulfate group.[91]

The experimental elastic neutron diffraction profile $S(\vec{Q})$ for α-Li_2SO_4 contains a large contribution from diffuse scattering. Also, the absence of high-order Bragg reflections indicates that center-of-mass displacements are substantial. Bragg scattering is determined by the

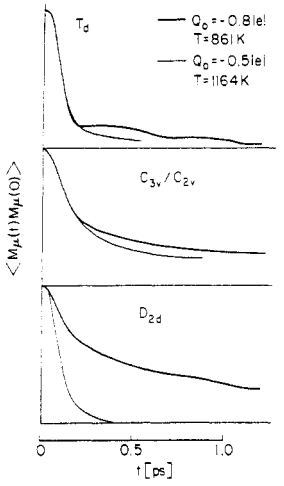

Figure 13. Orientational order parameter autocorrelation function for the two models for Li_2SO_4 discussed in the text. Note the slower decay of D_{2d} order for the model with Q_O = −0.8 e. Reprinted from ref 90; copyright 1985 American Institute of Physics.

structure amplitude $\langle\rho(\vec{Q},t)\rangle$ (cf. eq 17) and hence, by difference, diffuse scattering is related to $\langle[\delta\rho(\vec{Q},t)]^2\rangle$, the mean-square fluctuations in $\rho(\vec{Q},t)$. The calculated $S(\vec{Q})$ for the two model charge distributions indicates that, while diffuse scattering is very small for the model with Q_O = −0.5 e, the model with Q_O = −0.8 e yields a pattern in good agreement with experiment. Thus, the charge distribution of the molecular anion clearly plays a dominant role in determining the structure—and hence $S(\vec{Q})$—for this system.

The α phase of Li_2SO_4 is cubic, but on cooling below 848 K, the system transforms into the fully ordered monoclinic β phase. Using model II discussed above, Impey et al. investigated this transition in detail by using constant-pressure MD.[90] The interested reader is referred to the original article for a full account. The orientational dynamics of the SO_4^{2-} groups in the rotator phase can be described in terms of the time autocorrelation functions introduced earlier (cf. eq 31). These are shown in Figure 13 for the two models discussed above. The model with Q_O = −0.8 e results in D_{2d} order persisting much longer than with the other model. As in other examples, autocorrelation of atomic *velocities* now can be used to probe the translational dynamics. They are plotted in Figure 14 for the Li^+ and SO_4^{2-} ions, together with the corresponding phonon densities of states. Thus, Li^+ ions vibrate at frequencies mostly in the range 200–500 cm^{-1}, in agreement with Raman data, while the oscillations of the sulfate groups are centered about 100 cm^{-1}.

The time integral of $Z(t)$ is a measure of the self-diffusion constant, and it is found to differ significantly from zero in the case of Li^+ ions. A real-time graphics study demonstrates that the motion proceeds by jumps; i.e., Li^+ ions are localized for considerable periods of time and then rapidly move to another localized site. As in CaF_2, octahedral sites play a vital role in the diffusive motion.[92,93] The mean residence time of Li^+ ions on tetrahedral sites was estimated to be ≈5–10 ps, compared to a jump time of about 0.2 ps. These results agree well with the predictions of the Chudley–Elliot jump-diffusion model.[94] An attempt was also made at establishing a connection between diffusion jumps and SO_4^{2-} reorientations. However, because diffusion events

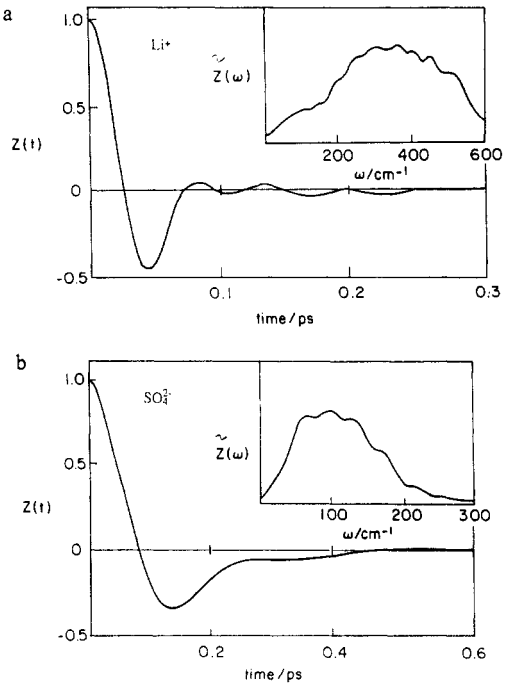

Figure 14. Velocity–velocity correlation function and corresponding power spectrum for Li^+ and SO_4^{2-} ions in model I for the α phase of Li_2SO_4. The low-frequency part of $\tilde{Z}(\omega)$ is uncertain due to truncation errors in the Fourier transform. Reprinted from ref 90; copyright 1985 American Institute of Physics.

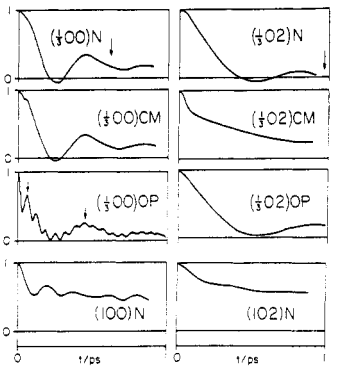

Figure 15. Intermediate scattering function $F(\vec{Q},t)$ for various $\vec{Q} = (2\pi/a)(l,m,n)$ wavevectors for model II of Li_2SO_4. N denotes neutron, CM center-of-mass (acoustic), and OP charge (optic) weighted dynamic structure factors. The left-hand column relates to longitudinal modes, and the right-hand column to transverse modes. Arrows for the N modes mark the vibrational periods measured by Brillouin scattering[96] while those for the longitudinal OP mode indicate the presence of a high-frequency LO phonon superimposed on a low-frequency LA phonon. Reprinted from ref 90; copyright 1985 American Institute of Physics.

are relatively rare in a simulation, it was not possible to draw definite conclusions.

Figure 15 shows several examples of the computed intermediate function $F(\vec{Q},t)$ for phonons propagating along the crystal [001] direction; longitudinal and transverse profiles are plotted side by side. Three types of correlation functions have been calculated. Those labeled N (neutron) use the correct neutron weights; those labeled CM set $b_{Li} = b_S = 1$ and $b_O = 0$; and those labeled OP employ $b_{Li} = +1$, $b_S = -1$, and $b_O = 0$. Indicated by arrows are the periods of vibration estimated from the Brillouin scattering measurements.[95] The calculated periods are too short, indicating that the model crystal is too stiff. Figure 15 shows that longitudinal acoustic (LA) modes, as exemplified by the

curves labeled (1/3,0,0)N and (1,0,0)N, are well defined, while transverse acoustic (TA) modes, (1/3,0,2)N and (1,0,2)N, are heavily damped. The nondecaying long-time component, which signals the presence of a strong central peak, is undoubtedly related to the extreme disorder in the crystal. Finally, the longitudinal optic (LO) correlation function (1/3,0,0)CP displays not only the high-frequency LO vibration but also the lower frequency LA mode. Hence, it is the optic modes that couple to the reorientations of the SO_4^{2-} molecules, as required by general symmetry arguments.[7,46]

C. The Mixed Cyanides

The mixed cyanides are site-disordered solid solutions where the anions or the cations randomly substitute for one another on their respective lattices. They can be mixtures of two alkali cyanides, such as $(RbCN)_{1-x}(KCN)_x$ and $(NaCN)_{1-x}(KCN)_x$, or of an alkali halide and an alkali cyanide, such as $(KCl)_{1-x}(KCN)_x$, $(NaCl)_{1-x}(NaCN)_x$, and—the most widely studied system in this family—$(KBr)_{1-x}(KCN)_x$.

At high temperatures, the mixed alkali halide–alkali cyanides possess overall cubic symmetry (space group $Fm3m$) with the CN^- ions undergoing rotational diffusion. As temperature is lowered, however, a remarkably intricate pattern of phases is revealed, the transitions often being accompanied by softening of transverse acoustic phonons (shear modes). In the *pure* cyanides, the first-order transition is primarily driven by the coupling of the translational to the rotational degrees of freedom of the aspherical CN^- molecules.[7,96] As replacement of the CN^- by halide ions proceeds, the presence of random strains increases. The coupling of these with the rotational motion of the cyanides plays a key role in establishing the ground-state structure of these systems. In fact, it has been demonstrated that the nature of the transition is determined by a *competition* between translation–rotation and strain–rotation couplings.[97] Theoretical studies yield similar conclusions.[98] Thus there exists in alkali halide–alkali cyanide mixtures a critical concentration x_c above which long-wavelength ferroelastic shear deformations dominate, thus causing a transition to a low-temperature noncubic structure with long-range orientational order. Below x_c, on the other hand, the inhomogeneous strains of the heavily diluted system take over the ferroelastic strains, thus causing the orientational order to be lost: the system freezes into an orientational glass state, the nature of which is not yet fully understood. Recent theoretical work by Michel[99] and Bostoen and Michel[100] suggests that the glass transition might result from a nonergodic instability, in a way analogous to that postulated for atomic glasses by mode-coupling theory.[101,102] A review of orientational glass formation in the cyanides has recently been given by Loidl.[103]

We begin with an overview of the structural phase diagram of the prototypical cyanide $(KBr)_{1-x}(KCN)_x$, emphasizing those aspects that MD simulations have helped elucidate. This is followed by a brief discussion of the dynamical properties of these materials.

1. Structural Transitions

On cooling from the high-temperature rotator phase, pure potassium cyanide undergoes a cubic → orthorhombic ferroelastic transition at 168 K, followed at 83 K by an antiferroelectric ordering transition.[104,105] The first of these transitions is anomalous, as phonons of T_{2g} symmetry exhibit dramatic softening; as noted earlier, translation–rotation coupling is thought to be responsible for this behavior. It suffices to add a few percent Br^-, however, in order for the ground state to depart from orthorhombic. For high cyanide concentrations, $0.85 \leq x \leq 1$, orthorhombic and triclinic phases are found to coexist.[106,107] For $0.6 \leq x \leq 0.85$, on the other hand, the ground-state structure is monoclinic, though a rhombohedral phase can also be present at intermediate temperatures.[106-109] Finally, in the Br^--rich regime, $x \leq 0.6 \equiv x_c$, the crystal remains cubic at all temperatures, even though a strong ferroelastic anomaly is seen in the dielectric, ultrasonic, and neutron responses. The latter has been interpreted as evidence for the formation of a quadruplar glass state.[46,110] It is generally accepted that, in these systems, dipolar (head-to-tail) and quadrupolar (orientational) freezing temperatures differ.[111,112]

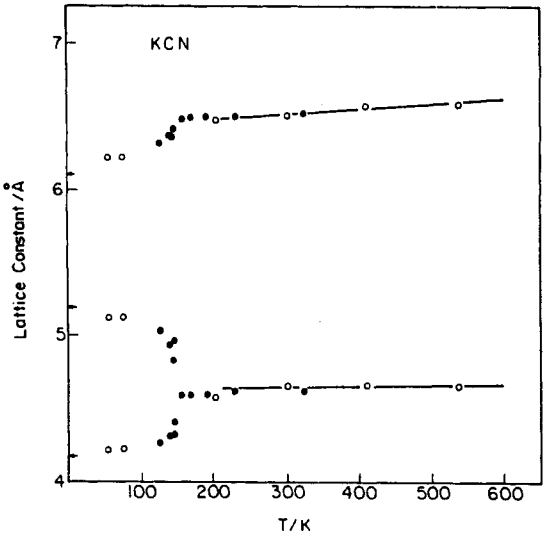

Figure 16. Molecular-dynamics simulation results for the temperature dependence of the lattice constants of pure KCN expressed in a body-centered tetragonal (bct) reference frame. In the high-temperature cubic rotator phase, the bct lattice constants are in a ratio $1/\sqrt{2}$:1. The bifurcation at low temperature signals the cubic → orthorhombic phase transition. The arrows show the low-temperature experimental lattice constants. Reprinted from ref 113; copyright 1985 American Institute of Physics.

In one of the earliest applications of the constant-pressure MD method, Impey, Klein, and Sprik investigated the cubic → orthorhombic transition in *pure* KCN.[113] In their study, the CN^- charge distribution was represented by a three-site model, with charges of −0.8 e at the N site, +0.8 e in the C–N bond a distance 0.204 Å from the C atom, and −e outside the C–N bond a distance 0.222 Å from the C atom. This model provides a reasonable representation of the essential higher order multipoles of the molecule.[114-118]

The system studied by Impey, Klein, and Sprik consisted of 216 ions ($N_+ = N_- = 108$). Figure 16 summarizes the simulation by a plot of the temperature dependence of the lattice parameters expressed in the appropriate body-centered tetragonal (bct) frame. Viewed in this reference frame, the high-temperature cubic phase is characterized by two lattice constants, in the ratio $1/\sqrt{2}$:1, as shown in Figure 16. At about $T = 140$ K, however, there is a bifurcation in the de-

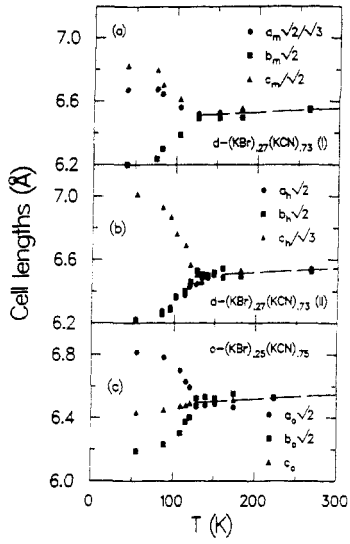

Figure 17. Temperature dependence of the cell lengths of three $(KBr)_{1-x}(KCN)_x$ mixtures, expressed in the appropriate ground-state reference frame: (a) Site-disordered $x = 0.73$ mixture, run I; ground state is monoclinic. (b) Site-disordered $x = 0.73$ mixture, run II; ground state is rhombohedral (here transformed to the corresponding hexagonal frame). (c) Site-*ordered* $x = 0.75$ mixture; ground state is orthorhombic. Cell lengths are scaled to yield the cubic lattice parameters at high temperature. Reprinted from ref 97; copyright 1986 American Institute of Physics.

generate bct constants a and b, accompanied by a marked reduction in the third parameter, c: in accord with experiment, the crystal has transformed from cubic to orthorhombic.

Encouraged by this success, an extensive series of simulations of the *mixed* system $(KBr)_{1-x}(KCN)_x$ was subsequently carried out by us using the *same* model.[97,119-123] A number of different samples were examined, most of them being comprised of 512 ions. The first was an investigation of the CN^--rich regime ($x \geq x_c$), with a sample containing 70 Br^- ions randomly distributed on the anion sublattice, d-$(KBr)_{0.27}$-$(KCN)_{0.73}$. Figure 17a displays the effect of isobarically cooling this system; here, we show only the cell lengths (the cell angles are not shown but, of course, have also been considered). Thus, between 127 and 105 K, the system clearly transforms to a structure of lower symmetry, which we recognize to be monoclinic. The observation of a low-temperature monoclinic phase accords well with experiment and is by itself a gratifying result, especially when we recall that the ground-state of *pure* KCN is orthorhombic. However, the monoclinic phase is experimentally preceded by a rhombohedral phase which forms at 112 K and whose range of existence is only about 4 K. Accordingly, a more careful study of the same site-disordered sample, this time using much smaller temperature intervals on cooling, was carried out. Results are shown in Figure 17b. Here, indeed, a cubic → rhombohedral transformation is now observed at ≈120 K, in excellent accord with experiment. Note that the latter phase persists down to the lowest temperatures; its energy is very close to that of the monoclinic phase and it is therefore not surprising that, once formed, it remains stable for the duration of the calculation.

In an attempt to understand the effect of random strains on the structure of these mixtures, a sample was studied in which the anions form an *ordered* A_3B pattern, o-$(KBr)_{0.25}(KCN)_{0.75}$. Results of these simulations

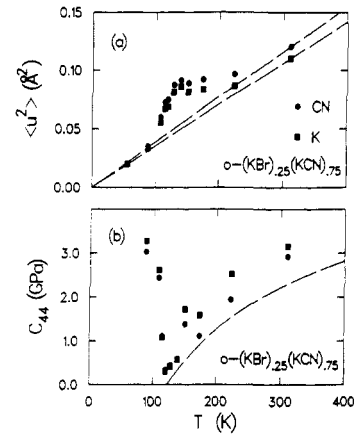

Figure 18. Temperature dependence of (a) the mean-square ionic displacement $\langle u^2 \rangle$ and (b) two independent estimates of the shear elastic constant c_{44} for run c of Figure 17. The dashed curves show in (a) the expected classical linear behavior and in (b) the mean-field fit to experimental results.[109] Reprinted from ref 97; copyright 1986 American Institute of Physics.

are shown in Figure 17c. Now, a transformation from the cubic rotator phase to an antiferro-ordered *orthorhombic* structure was observed—just as in *pure* KCN. These observations suggest that, in site-disordered samples, random strains are important in destabilizing the orthorhombic phase. Similar investigations of related systems support these conclusions.[120,123]

Corresponding studies were also performed on samples with cyanide concentrations less than the critical concentration x_c (=0.6 for this system), namely, $x = 0.5$ and 0.25. We do not show the results here but note that, consistent with experiment, both systems were observed to remain cubic at all temperatures.

As discussed earlier, while systems with $x \geq x_c$ form an orientational *crystal* at low temperature, systems with $x < x_c$ freeze into an orientational *glass* state, the nature of which is not fully understood. The dramatic softening of the shear elastic constant c_{44} at the transition has been interpreted as evidence for the presence of critical fluctuations of T_{2g} symmetry, leading to a divergent mean-square displacement at T_c.[108,109] Thus, the crystal "melts" at the transition. It is usually argued that, at this point, the system has two options: either (i) recrystallize ferroelasticity into a phase of lower symmetry for $x \geq x_c$ or (ii) freeze its disorder into an orientational glass phase of overall cubic symmetry for $x < x_c$. We have however demonstrated that *noncubic* orientational glass phases may develop in heavily strained systems such as $(KCl)_{1-x}(KCN)_x$.[120]

Figure 18 shows the calculated temperature dependence of the mean-square displacement, $\langle u^2 \rangle$, and that of the shear elastic constant, c_{44}, for the system with ordered A_3B anion sublattice. In the neighborhood of the transition, $\langle u^2 \rangle$ clearly departs from the classical linear temperature dependence (indicated by the dashed lines). At the ferroelastic transition temperature, which is an order of magnitude smaller than the melting temperature, we find that *Lindemann's criterion is satisfied.* This anomalous behavior is accompanied by a dramatic softening of c_{44}, as shown in Figure 18b. The departure between calculated and measured c_{44} (dashed line) is most likely related to the finite size of the system.

In order to better understand the orientational freezing transition, we have examined the quantity

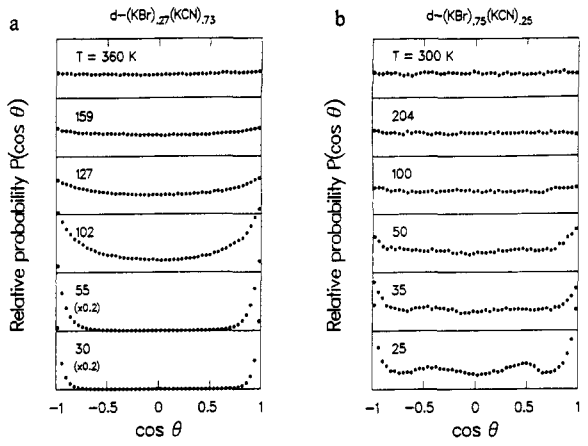

Figure 19. Evolution as a function of temperature of $P(\cos\theta)$, the relative probability of finding a pair of neighboring molecules such that θ is the angle between them, for the $(KBr)_{0.27}(KCN)_{0.73}$ and $(KBr)_{0.75}(KCN)_{0.25}$ site-disordered mixtures. Note that the lowest two panels have been scaled down by a factor of 5 for the sample with $x = 0.73$. Reprinted from ref 119; copyright 1987 American Chemical Society.

$P(\cos\theta)$, which gives the relative probability of finding a pair of neighboring CN^- molecular ions such that θ is the angle between them. The temperature dependence of $P(\cos\theta)$ is plotted in Figure 19 for the two site-disordered systems discussed above. At high temperature, both samples exhibit rotational diffusion, the molecules interacting with one another only weakly: there is no preferred orientation, and the distribution is flat. As cooling proceeds, however, both systems develop a tendency for neighboring molecules to align parallel ($\cos\theta = +1$) or antiparallel ($\cos\theta = -1$). This behavior is unequivocal in the $(KBr)_{0.27}(KCN)_{0.73}$ sample (Figure 19a): at the lowest temperature examined, the quadrupoles have *completely* ordered in a ferroelastic pattern, i.e., with their axes parallel but with head-to-tail disorder. The $(KBr)_{0.75}(KCN)_{0.25}$ sample, on the other hand, behaves differently (Figure 19b): even though quadrupolar alignment is preferred, there exists at low temperature a broad featureless distribution of relative orientations. This suggests a picture of the orientational glass state as consisting of CN^- molecular ions loosely aligning along preferred directions, while exhibiting a definite tendency toward ferroelastic ordering. Interestingly, antiferroelastic ordering ($\cos\theta = 0$) is *not* a favored configuration.

It is quite remarkable that such a simple model—two-body potentials and a three-site charge distribution for the CN^- molecular ions—is able to reproduce virtually the whole phase diagram of such a complex mixed crystal system. The MD studies have yielded numerous insights into the effect of both site disorder and orientational disorder. We now turn to a discussion of the dynamical properties of these materials.

2. Dynamical Properties

Single-particle dynamics can be studied by computing a number of time correlation functions relevant to polarized Raman scattering experiments, a powerful experimental probe of such systems. As an extension of the approach used by Edwards and Anderson to characterize magnetic impurities in spin glasses,[124] one examines time-dependent correlations in quantities of the form $Y(\hat{u})$, where $\hat{u} \equiv (x,y,z)$ is the unit vector along the

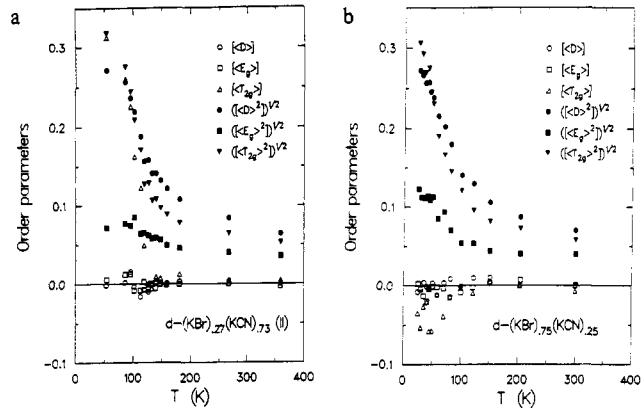

Figure 20. Temperature dependence of the CN^- orientational order parameters and their fluctuations for the $(KBr)_{0.27}(KCN)_{0.73}$ and $(KBr)_{0.75}(KCN)_{0.25}$ site-disordered mixtures. Reprinted from ref 119; copyright 1987 American Chemical Society.

C–N bond, using the cubic crystal axes as a reference. Dipolar (D) order is monitored through the three functions of T_{1u} symmetry

$$Y_1^{(1)} = \left(\frac{3}{4\pi}\right)^{1/2} x$$

$$Y_2^{(1)} = \left(\frac{3}{4\pi}\right)^{1/2} y \qquad (32)$$

$$Y_3^{(1)} = \left(\frac{3}{4\pi}\right)^{1/2} z$$

whereas quadrupolar order is described via two functions of E_g symmetry

$$Y_1^{(2)} = \left(\frac{15}{4\pi}\right)^{1/2} (3z^2 - 1)$$

$$Y_2^{(2)} = \left(\frac{15}{4\pi}\right)^{1/2} (x^2 - y^2) \qquad (33)$$

and three functions of T_{2g} symmetry

$$Y_3^{(2)} = \left(\frac{15}{4\pi}\right)^{1/2} xy$$

$$Y_4^{(2)} = \left(\frac{15}{4\pi}\right)^{1/2} yz \qquad (34)$$

$$Y_5^{(2)} = \left(\frac{15}{4\pi}\right)^{1/2} zx$$

First we show, in Figure 20, the temperature dependence of the time-averaged $Y(\hat{u})$'s and their fluctuations for the two site-disordered systems considered above. From the behavior of the fluctuations, it is clear that, at low temperature, the sample with $x = 0.73$ (Figure 20a) has CN^- orientations frozen into the {111} directions. Examination of the other order parameters reveals that *only* the [111] and $[\bar{1}\bar{1}\bar{1}]$ directions are occupied; i.e., *all* C–N bond vectors align parallel to the [111] direction of the parent cubic phase, consistent with our earlier findings. The situation is somewhat different in the sample with $x = 0.25$ (Figure 20b), where again the C–N axes align along the {111} directions, but only in an *average* sense, that is, with a wide distribution of orientations.

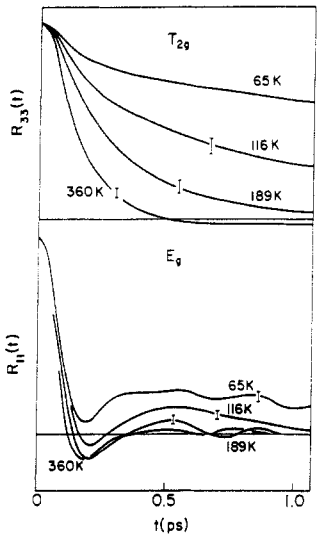

Figure 21. Autocorrelation functions for the order parameters appropriate to Raman scattering in $(KBr)_{0.5}(KCN)_{0.5}$ at various temperatures. Vertical lines give a measure of the uncertainty in the calculation. Reprinted from ref 125; copyright 1982 Taylor & Francis Inc.

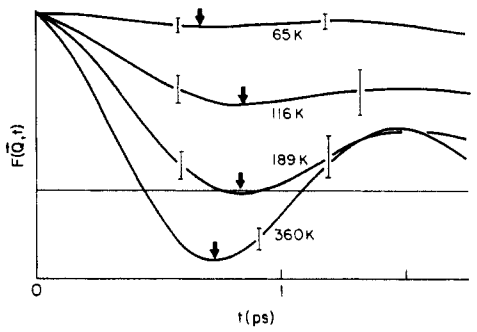

Figure 22. Intermediate scattering function $F(\vec{Q},t)$ for the transverse acoustic phonon with wavevector $(2\pi/a)(1/3,0,1)$ in $(KBr)_{0.5}(KCN)_{0.5}$ at various temperatures. Arrows mark the half-period of oscillation, and error bars give an indication of the error in the MD data. Reprinted from ref 125; copyright 1982 Taylor & Francis Inc.

Time-dependent orientational correlations are studied via the two functions

$$R_{11}(t) = \langle Y_1^{(2)}(t) Y_1^{(2)}(0) \rangle \quad (E_g) \tag{35}$$

and

$$R_{33}(t) = \langle Y_3^{(2)}(t) Y_3^{(2)}(0) \rangle \quad (T_{2g}) \tag{36}$$

These are shown in Figure 21 for a system with $x = 0.5$.[125] The E_g function, though strongly damped, has an oscillatory behavior at short times which is likely the signature of librational motion of the CN^- molecule. The oscillation persists down to the lowest temperature examined, and the main consequence of reducing the temperature is the appearance of a marked long-time tail. By contrast, the T_{2g} function is only weakly negative at 360 K, while it is purely diffusive in character at lower temperatures. The decay time of $R_{33}(t)$ increases rapidly as temperature is lowered; it is about 4 ps at 65 K.

Turning to collective modes now, Rowe et al. have measured the dynamic structure factor for the mixed crystal $(KBr)_{0.5}(KCN)_{0.5}$ at values of $\vec{Q}$ corresponding to a number of different branches of the phonon dispersion curves.[110] Of particular interest is the [001] transverse acoustic mode, since this is the one that exhibits dramatic softening at the transition. Figure 22 shows the intermediate scattering function $F(\vec{Q},t)$ at $\vec{Q} = (2\pi/a)(1/3,0,1)$ as obtained by Bounds et al. in a MD simulation.[125] At high temperature, there is a well-defined oscillation. As temperature is reduced, however, the envelope of the function lengthens greatly, corresponding to the growth of a strong central peak in $S(\vec{Q},\omega)$. In addition, it is clear that as temperature is lowered, the position of the minimum first shifts to longer times (i.e., lower frequencies), corresponding to the mode softening behavior discussed in section 1, and then recovers.

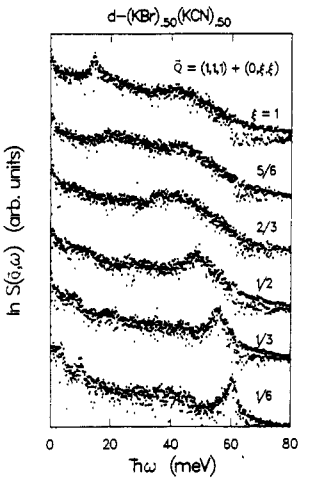

Figure 23. Dynamic structure factor $S(\vec{Q},\omega)$ (in arbitrary units) for phonons propagating along the [011] direction at six different points in the zone for a $(KBr)_{0.5}(KCN)_{0.5}$ model containing 1728 particles at 25 K (after Lewis and Klein, unpublished).

Recently, a more detailed study was undertaken of the dynamical properties of the mixed system $(KBr)_{0,5}(KCN)_{0,5}$, but now using a much larger sample comprised of $N = 1728$ particles. Because of the prohibitive demands of computation time of such a large simulation, the system was examined at only one temperature, namely, $T = 25$ K, which is below the orientational freezing temperature. Figure 23 shows the total dynamic structure factor for six different and equidistant wavevectors along the [011] direction. The sharp peak at small momentum transfer and high frequency is identified as a longitudinal optic mode, whose dispersion with increasing wavevector is readily apparent. The two barely resolved low-frequency peaks are likely due to the transverse acoustic phonon and a librational mode. (The latter is identified with the aid of the E_g correlation function of Figure 21.) These peaks merge as the momentum transfer increases. Figure 23 thus provides a graphic illustration of a neutron scattering profile calculation that can be carried out with present-day computers.

D. Calcium/Potassium Nitrates and the Glass Transition

There has been considerable interest recently in the dynamics of nitrate crystals. A molecular-dynamics study of several of the phases of solid KNO_3 was reported recently,[126] while a computer investigation of the nature of the disorder in the high-temperature phase of $NaNO_3$ was also carried out.[127] The main thrust of experimental activity,[128-131] however, has been directed toward an understanding of the glass transition in the fused salt $[Ca(NO_3)_2]_{0.4}[KNO_3]_{0.6}$—a material with ex-

cellent glass-forming ability. The relative simplicity of the constituent species in this so-called "fragile" liquid[131] makes it an ideal candidate for a detailed study by molecular dynamics. Such a study of structural relaxation and dynamical correlations was recently reported by Signorini, Barrat, and Klein;[132] we devote the remainder of this section to a discussion of this calculation.

Recent theories of supercooled liquids,[101,102,133] such as those based on the mode-coupling approximation, describe the glass transition as an ideal ergodic to nonergodic transition occurring at a well-defined temperature; this transition is triggered by the nonlinear feedback mechanism governing the relaxation of density fluctuations and is smeared by the existence of activated processes that restore ergodicity on a long time scale. Besides the existence of such a transition, mode-coupling theories predict the appearance of two different slow relaxation contributions to the time-dependent correlation functions close to the transition, the so-called α (primary) and β (secondary) relaxation mechanisms. Both α relaxation and β relaxation are predicted to slow down critically when the transition temperature T_c is approached.[101,102] A number of theoretical predictions have been confirmed—at least qualitatively—by neutron scattering experiments[134-136] and computer simulations on simple models.[65,137-139] The large time window explored by time-of-flight and spin–echo neutron scattering experiments[134-136] allows a detailed analysis of the scaling behavior near the transition. Although a comparable time range cannot yet be explored with MD, such calculations can nevertheless yield valuable insights on the nature of microscopic dynamical processes in glassy systems.[140]

The system considered by Signorini, Barrat, and Klein[132] consisted of 192 K^+, 128 Ca^{2+}, and 448 NO_3^- ions contained in a periodically replicated cubic box and interacting via atom–atom and charge–charge potentials of the Buckingham (Tosi–Fumi[35]) type. The cations carried their full charges, and the NO_3^- ion was treated as a rigid unit with fractional charges on the N and O atoms; no polarizability effects were considered. The study of the glass transition was initiated with a sequence of cooling–equilibration–run cycles, carried out under constant-temperature, constant-pressure conditions,[13,14] which eventually brought the system temperature to 700, 600, 550, 450, and 350 K, respectively. Note that because of the presence of long-range Coulombic interactions, which require excessively long calculation times, the effective cooling rate had to be rather high.

Figure 24 shows a comparison between the phonon density of states as obtained from time-of-flight measurements[134] and from Fourier inverting the calculated velocity autocorrelation function. Apart from a high-frequency shoulder which is absent in the calculation, the model reproduces correctly the broad features of the phonon spectrum.

1. Structure of the Glass

The structure of the system at different temperatures was monitored in terms of the partial pair distribution functions $g_{ij}(r)$, an example of which is given in Figure 25. The calculation reveals that the basic liquid-like structure is preserved when the fused salt is cooled. In

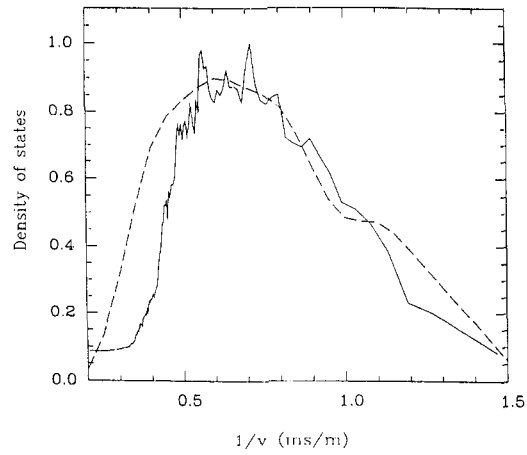

Figure 24. Phonon density of states (in arbitrary units) for glassy $[Ca(NO_3)_2]_{0.4}[KNO_3]_{0.6}$ plotted as a function of the inverse velocity of the scattered neutrons in a time-of-flight experiment; the full curve is the neutron-weighted power spectrum constructed from the atomic velocity autocorrelation function, while the dashed curve is the experimental result of Mezei, Knaak, and Farago.[134] Reprinted from ref 132; copyright 1989 American Institute of Physics.

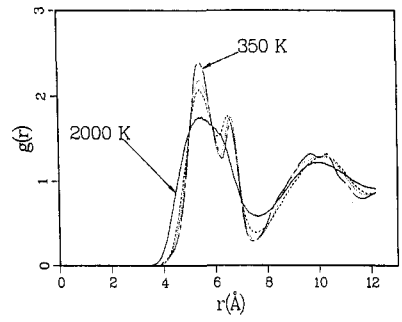

Figure 25. Radial distribution function for Ca^{2+}–Ca^{2+} correlations at various temperatures: 2000 K (full), 800 K (dashed), 550 K (dots), and 350 K (long dashes), respectively; note the split first peak. Reprinted from ref 132; copyright 1989 American Institute of Physics.

particular, the peak positions in $g_{ij}(r)$ suffer only slight shifts as temperature and volume decrease, while the main peaks remain fairly broad at all temperatures. The distribution functions for Ca–O and Ca–N reveal an alternating pattern of negatively and positively charged shells characteristic of molten salts. The area under the nearest-neighbor Ca–O and Ca–N peaks indicates that NO_3^- is, on average, surrounded by 2.2 Ca^{2+} ions, with the Ca–N vector forming a small angle (ca. 20°) with the molecular plane. The $g(r)$ for K–N and K–O pairs at the same temperature yields a coordination number of 7.5 K^+ around each NO_3^-, but with a much less well-defined structure. The function $g_{Ca-Ca}(r)$ (Figure 25) is perhaps more interesting, as it shows the nearest-neighbor peak to split at low temperatures. Though this feature, because it is already present at 800 K, cannot be directly related to the onset of the glassy phase, a detailed analysis indicates that it arises from the existence of two preferred arrangements for the Ca^{2+} ions closest neighbor to a given NO_3^- molecule: essentially, the two Ca^{2+} ions can sit either on the same side or on opposite sides of the NO_3^- molecular plane.

2. Diffusion

A rough estimate of the diffusion processes can be obtained by examining the atomic mean-square dis-

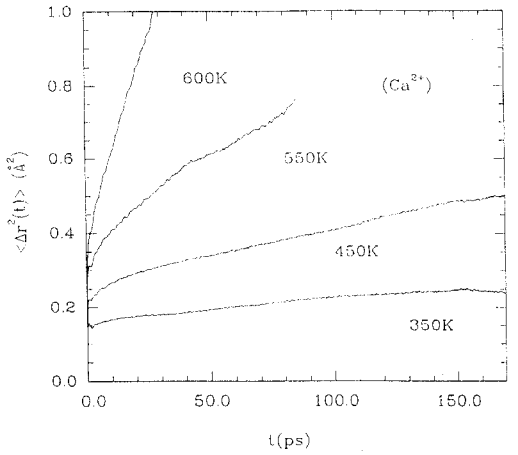

Figure 26. Mean-square displacements of Ca^{2+} ions as a function of time at various temperatures; the slope of each curve is a measure of the diffusion constant at that temperature. Reprinted from ref 132; copyright 1989 American Institute of Physics.

placements as a function of temperature, the slope of which yields the diffusion constant D (cf. eqs 23 and 24). Figure 26 shows $\langle \Delta r^2(t) \rangle = \langle |\vec{r}(t) - \vec{r}(0)|^2 \rangle$ for the Ca^{2+} ions. The diffusion constant clearly decreases rapidly with T, though it does not vanish even at the lowest temperature examined.

A more detailed picture of this mechanism, however, is provided by the *self* part of the van Hove correlation function, $G_s(r,t)$, obtained from eq 15 by restricting the double summation to terms with $i = j$. In a liquid, $G_s(r,t)$ relaxes to 0 for long times, asymptotically reaching a Gaussian shape of width Dt. In a solid, $G_s(r,t)$ levels off to a finite value at long times, the width now being related to the Lindemann ratio. Figure 27 presents results for the self-diffusion of Ca^{2+} ions at different temperatures. The maximum in $r^2G_s(r,t)$ is a measure of the most probable position of a particle at time t, given that it was at the origin at $t = 0$. At $T = 600$ K, this maximum is clearly drifting with increasing times, indicating liquid-like structure. At $T = 350$ K, on the other hand, the results reveal behavior characteristic of a system in a state of "structural arrest"—at least on the time scale of the simulation. The other species display similar behavior, except for oxygen, whose $G_s(r,t)$ possesses a peculiar double-peaked structure, as shown in Figure 28, due to the rotational motion of the nitrate ions. This feature was found to be present at all temperatures. The above results for $\langle \Delta r^2(t) \rangle$ and $G_s(r,t)$ therefore yield an estimate of 400 K for the temperature at which the system passes from a state of ergodicity (liquid-like) to one of nonergodicity (glass-like), i.e., for the glass transition temperature.

3. Structure Factors and Scaling

The spatial Fourier transform of $G_s(r,t)$ yields the structure factor for incoherent neutron scattering (cf. eq 18). In a simulation, this quantity can be obtained with much better accuracy than in an experiment. For atomic systems and for wavevectors near the first peak in the structure factor, k_0, both coherent and incoherent responses display a similar time dependence. Accordingly, it is possible to compare the total neutron scattering intensity with the response for Ca^{2+} ions only—rather than with the actual average weighted over all species.

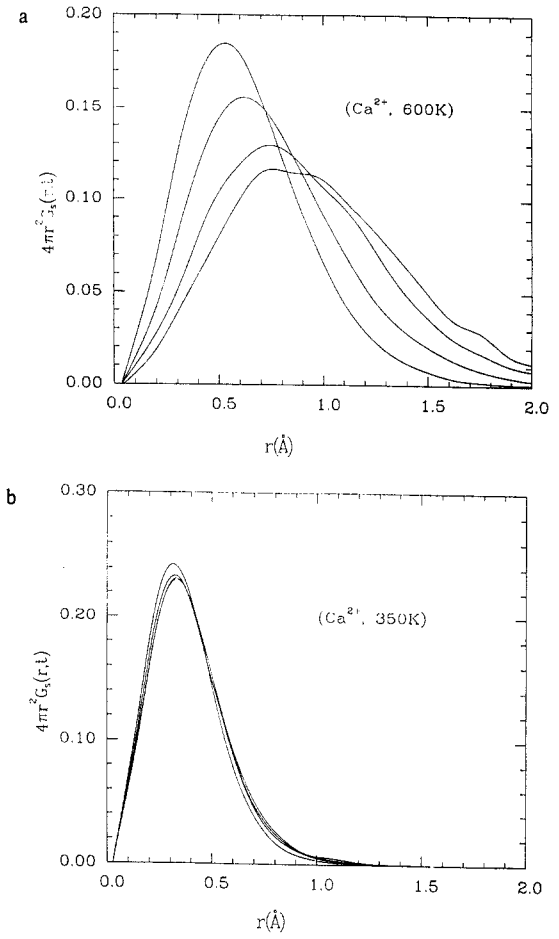

Figure 27. Self-part of the real-space van Hove correlation function for Ca^{2+} ions at (a) 600 K for times $t = 5$, 15, 30, and 45 ps, respectively, and (b) 350 K, $t = 10$, 60, 120, and 280 ps, respectively. Reprinted from ref 132; copyright 1989 American Institute of Physics.

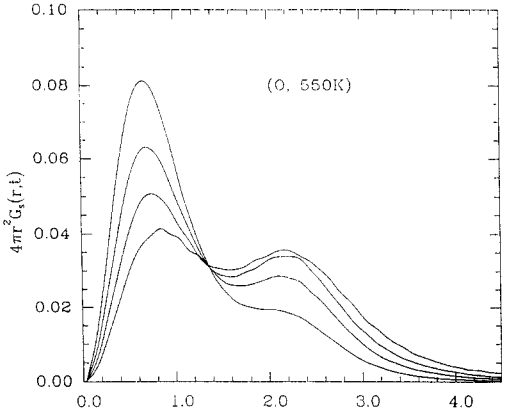

Figure 28. Self-part of the real-space van Hove correlation function for oxygen atoms at 550 K for times $t = 10$, 30, 60, and 90 ps, respectively. Reprinted from ref 132; copyright 1989 American Institute of Physics.

Figure 29 shows the calculated $F_s(k_0,t)$ for Ca^{2+} ions at $k_0 = 1.74$ Å^{-1}, which can be compared with the neutron results displayed in Figure 3 of ref 134. Three relaxation modes are clearly visible: The first, almost independent of temperature, occurs on a time scale $t \leq 0.5$ ps, typical of inverse phonon frequencies. The second mode is characterized by a positive curvature of $F_s(k_0,t)$ in a semilog plot, which becomes more pronounced as T decreases. This feature can be identified with β relaxation processes. The third mode finally

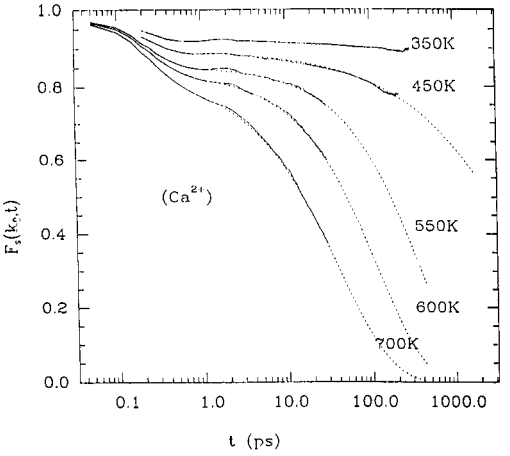

Figure 29. Temperature dependence of $F_s(k_0,t)$ for Ca^{2+} ions at $k_0 = 1.74$ Å^{-1}; the dashed lines show the fitted curves used to extrapolate the data. Reprinted from ref 132; copyright 1989 American Institute of Physics.

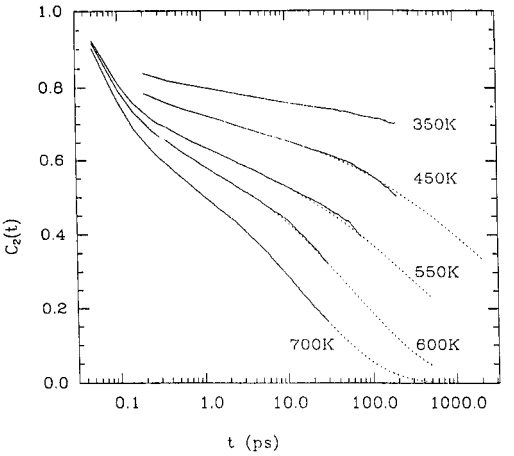

Figure 30. Temperature dependence of the orientational relaxation function $C_2(t)$; the dashed lines show the fitted curves used to extrapolate the data. Reprinted from ref 132; copyright 1989 American Institute of Physics.

slows down considerably when temperature decreases and corresponds to the α relaxation. It appears in the simulations at high temperature, but only its very beginning is discernible at $T = 450$ K.

These results now can be used to assess the scaling features of the α relaxation process, both predicted by mode-coupling teory[102] and observed experimentally.[136] Indeed, a master curve $f(x)$ was obtained having the form

$$F_s(k_0,t;T) \equiv f(x) = f[t/\tau(T)] \tag{37}$$

where f is well approximated by the Kohlrausch law:

$$f(x) = 0.90 \exp(-x^{0.61}) \tag{38}$$

As expected, the temperature-dependent relaxation times $\tau(T)$ that appear in the fit are of the same order of magnitude as typical diffusion times. On the other hand, the fact that the results for $T = 350$ K do not lie on the master curve indicates that, at this state point, the system is glassy in character.[138]

4. Orientational Relaxation

An analysis of the $G_s(r,t)$ plot for the oxygen atoms (Figure 28) revealed the existence of an important reorientational motion of the NO_3^- ions at all temperatures. A more detailed picture of this motion is provided by the distribution function for the tilt angle of the molecular plane, $\theta(t)$, defined as

$$\theta(t) = \cos^{-1}[\vec{u}(t)\cdot\vec{u}(0)] \tag{39}$$

Here, $\vec{u}(t)$ is a unit vector perpendicular to the molecular plane at time t. The appropriate distribution function $G(\theta,t)$ can then be expanded in terms of Legendre polynomials

$$G(\theta,t) = \sum_l C_l(t)P_l(\cos\theta) \tag{40}$$

where

$$C_l(t) = \langle P_l(\cos\theta(t))\rangle \tag{41}$$

In the case of diffusive reorientational motion, $C_l(t) \approx \exp(-t/\tau_l)$, with $\tau_l = \tau_0/[l(l+1)]$. Though the results are not shown, the MD data reveal that a slow diffusive motion takes place at high temperature, together with larger angular jumps that populate the region between $\pi/2$ and π. As the temperature is lowered, angular diffusion slows down, and at 350 K, reorientations occur almost exclusively through jumps of amplitude close to π. The data clearly show the freezing of diffusion and the predominance of large-amplitude jumps at 350 K. An analysis of the motion of N–O bond vectors at this temperature indicates that the jumps involve mainly rotations about twofold axes. Jump motion about the threefold axis was also observed in the glass but is much less prevalent.

A measure of the time scale of molecular reorientations can be obtained from a study of the relaxation of the coefficients $C_1(t)$ and $C_2(t)$ defined in eq 41. The latter, displayed in Figure 30, exhibits the same three-mode structure found for $F_s(k_0,t)$. The α, or long-time branches of the functions $C_1(t)$ and $C_2(t)$, can also be fitted to a Kohlrausch law, viz., $C_1(t) = 0.89 \exp[-(t/\tau_1)^{0.61}]$ and $C_2(t) = 0.76 \exp[-(t/\tau_2)^{0.42}]$. At 600 K and above, the predominance of large angular jumps is reflected in the value of the ratio τ_1/τ_2, which is close to 1, as predicted for this type of relaxation,[141] in contrast to the value of 3 associated with diffusive behavior. As the temperature is lowered, the most probable motion involves rotational jumps of about π; hence the relaxation of $C_2(t)$—which is unaffected by instantaneous flips of π—slows down more rapidly than that of $C_1(t)$ and the ratio τ_2/τ_1 tends to diverge.

Experimentally, the rotational motion of NO_3^- ions has been investigated by conventional Raman scattering.[142] Below the glass transition, the polarized and depolarized Raman lines of a totally symmetric intramolecular vibrational band can be superimposed, within the experimental resolution, indicating that orientational relaxation in the glass is occurring on a time scale longer than about 100 ps. This finding is in broad agreement with the simulation results discussed above. Recent Brillouin scattering data have been interpreted to indicate that rotational and translational motions decouple near the glass transition.[128] However, the MD calculations discussed here do not seem to support this suggestion. More precisely, the apparent decoupling observed between the relaxation times for $C_1(t)$ and $C_2(t)$ was explained simply by the existence of thermally activated flips of anion molecular planes. These flips

persist at low temperature but, in a first approximation, should not affect the Brillouin intensities. Most recent studies using picosecond light scattering suggest that the Kohlrausch exponent is temperature dependent.[143]

V. Concluding Remarks

We have reviewed a selection of the many applications of molecular dynamics to the study of molecular solids as generated over the past two decades, drawing heavily from our own studies of ionic molecular solids. The phenomena we have considered have mostly been connected with dynamical behavior, although it is inevitable that in the more complex systems, structural aspects were also discussed. From the range of examples presented, it is evident that the technique of molecular dynamics has now evolved to the point of becoming a powerful complement to real experiments in the study of the dynamical behavior of molecular crystals. The coming years will clearly see the role of such simulations increase greatly, particularly in the study of complex materials. Other papers in this issue give ample evidence that simulation methods now form part of mainstream chemistry.

References

(1) Alder, B. J.; Wainwright, T. E. *J. Chem. Phys.* **1957**, *27*, 1208.
(2) Rahman, A. *Phys. Rev.* **1964**, *136*, A405.
(3) Gibson, J. B.; Goland, A. N.; Milgram, M.; Vineyard, G. H. *Phys. Rev.* **1960**, *120*, 1229.
(4) Koehler, T. R. In *Dynamical Properties of Solids*; Horton, G. K., Maradudin, A. A., Eds.; North-Holland: Amsterdam, 1975; Vol. 2, Chapter 1.
(5) Barron, T. H. K.; Klein, M. L. In *Dynamical Properties of Solids*; Horton, G. K., Maradudin, A. A., Eds.; North-Holland: Amsterdam, 1974; Vol. 1, Chapter 7.
(6) Horner, H. In *Dynamical Properties of Solids*; Horton, G. K.; Maradudin, A. A., Eds.; North-Holland: Amsterdam, 1974; Vol. 1, Chapter 8.
(7) Michel, K. H.; Rowe, J. M. *Phys. Rev. B* **1985**, *32*, 5827.
(8) Briels, W. J.; Jansen, A. P. J.; van der Avoird, A. *Adv. Quantum Chem.* **1986**, *18*, 131.
(9) Ciccotti, G.; Hoover, W. G., Eds. *Molecular-Dynamics Simulation of Statistical-Mechanical Systems*; Proceedings of the International School of Physics "Enrico Fermi"; North-Holland: Amsterdam, 1986.
(10) Allen, M. P.; Tildesley, D. J. *Computer Simulation of Liquids*; Clarendon Press: Oxford, 1987.
(11) Ciccotti, G.; Frenkel, D.; McDonald, I. R., Eds. *Simulation of Liquids and Solids*; North Holland: Amsterdam, 1987.
(12) Parrinello, M.; Rahman, A. *Phys. Rev. Lett.* **1980**, *45*, 1196.
(13) Nosé, S.; Klein, M. L. *J. Chem. Phys.* **1983**, *78*, 6928.
(14) Nosé, S.; Klein, M. L. *Mol. Phys.* **1983**, *50*, 1055.
(15) Car, R.; Parrinello, M. *Phys. Rev. Lett.* **1985**, *55*, 2471.
(16) Allan, D. C.; Teter, M. P. *Phys. Rev. Lett.* **1987**, *59*, 1136.
(17) Needels, M.; Payne, M. C.; Joannopoulos, J. D. *Phys. Rev. Lett.* **1987**, *58*, 1765.
(18) Ballone, P.; Andreoni, W.; Car, R.; Parrinello, M. *Phys. Rev. Lett.* **1988**, *60*, 271.
(19) Car, R.; Parrinello, M. *Phys. Rev. Lett.* **1988**, *60*, 204.
(20) Galli, G.; Martin, R. M.; Car, R.; Parrinello, M. *Phys. Rev. Lett.* **1989**, *62*, 555; *Phys. Rev. Lett.* **1989**, *63*, 988.
(21) Li, X.-P.; Allen, P. B.; Car, R.; Parrinello, M. In *Atomic-Scale Calculations in Materials Science*; Tersoff, J., Vanderbilt, D., Vitek, V., Eds.; Materials Research Society Proceedings No. 141; Materials Research Society: Pittsburgh, 1989. Li, X.-P. *Phys. Rev. B* **1990**, in press.
(22) Buda, F.; Chiarotti, G. L.; Car, R.; Parrinello, M. *Phys. Rev. Lett.* **1989**, *63*, 294. Stich, I.; Car, R.; Parrinello, M. *Phys. Rev. Lett.* **1989**, *63*, 2240.
(23) Fernando, G. W.; Qian, G.-X.; Weinert, M.; Davenport, J. W. *Phys. Rev. B* **1989**, *40*, 7985. Qian, G.-X.; Weinert, M.; Fernando, G. W.; Davenport, J. W. *Phys. Rev. Lett.* **1990**, *64*, 1146.
(24) LeSar, R. *Phys. Rev. Lett.* **1988**, *61*, 2121.
(25) Swope, N. C.; Andersen, H. C. *Phys. Rev. B* **1990**, in press.
(26) Abraham, F. F. *Adv. Phys.* **1986**, *35*, 1.
(27) Andersen, H. C.; Allen, M. P.; Bellemans, A.; Board, J.; Clarke, J. H. R.; Ferrario, M.; Haile, J. M.; Nosé, S.; Opheusden, J. V.; Ryckaert, J.-P. *New Molecular Dynamics Methods for Various Ensembles*; Rapport d'activité scientifique du CECAM, 1984, p 82.
(28) Andersen, H. C. *J. Chem. Phys.* **1980**, *72*, 2384.
(29) Hoover, W. G.; Ladd, A. J. C.; Moran, B. *Phys. Rev. Lett.* **1982**, *48*, 1818.
(30) Evans, D. J. *J. Chem. Phys.* **1983**, *78*, 3297.
(31) Nosé, S. *Mol. Phys.* **1984**, *52*, 255; *J. Chem. Phys.* **1984**, *81*, 511.
(32) Nosé, S. *Mol. Phys.* **1986**, *57*, 187.
(33) van Hove, L. *Phys. Rev.* **1954**, *95*, 249.
(34) Hansen, J.-P.; McDonald, I. R. *Theory of Simple Liquids*, 2nd ed.; Academic Press: London, 1986.
(35) Tosi, M. P.; Fumi, F. G. *J. Phys. Chem. Solids* **1964**, *25*, 45. Fumi, F. G.; Tosi, M. P. *J. Phys. Chem. Solids* **1964**, *24*, 31.
(36) Maitland, G. C.; Rigby, M.; Smith, E. B.; Wakeham, W. A. *Intermolecular Forces: Their Origin and Determination*; Clarendon Press: Oxford, 1981.
(37) Price, S. L.; Stone, A. J. *J. Chem. Phys.* **1988**, *88*, 3325.
(38) Cochran, W.; Dick, B. G.; Overhauser, A. W. *Phys. Rev.* **1958**, *112*, 90; *Adv. Phys.* **1958**, *9*, 387; *Adv. Phys.* **1958**, *10*, 401.
(39) Sprik, M.; Klein, M. L. *J. Chem. Phys.* **1988**, *89*, 7556.
(40) Ryckaert, J.-P.; Bellemans, A. *J. Chem. Soc., Faraday Trans.* **1978**, *66*, 95.
(41) Ryckaert, J.-P.; Cicotti, G.; Berendsen, H. J. C. *J. Comput. Phys.* **1977**, *23*, 327.
(42) Fowler, P. W.; Klein, M. L. *J. Chem. Phys.* **1986**, *85*, 3913.
(43) Califano, S.; Schettino, V.; Netto, N. *Lattice Dynamics of Molecular Crystals*; Springer-Verlag: Berlin, 1981.
(44) Schneppe, O.; Jacobi, N. *Adv. Chem. Phys.* **1972**, *22*, 205.
(45) van den Berg, T. H. M.; van der Avoird, A. *J. Phys.: Condens. Matter* **1989**, *1*, 4047.
(46) Michel, K. H.; Rowe, J. M. *Phys. Rev. B* **1980**, *22*, 1417.
(47) de Raedt, B.; Michel, K. H. *Faraday Discuss. Chem. Soc.* **1980**, *69*, 88.
(48) Scott, T. A. *Phys. Rep.* **1976**, *27*, 89.
(49) LeSar, R. *J. Chem. Phys.* **1984**, *81*, 5104.
(50) Schiferl, D.; LeSar, R.; Moore, D. S. In *Simple Molecular Systems at Very High Density*; Polian, A., Loubeyre, P., Boccara, N., Eds.; Plenum: New York, 1989.
(51) Raich, J. C.; Gillis, N. S.; Anderson, A. B. *J. Chem. Phys.* **1974**, *61*, 1399.
(52) Raich, J. C.; Gillis, N. S.; Koehler, T. R. *J. Chem. Phys.* **1974**, *61*, 1411.
(53) Raich, J. C.; Mills, R. L. *J. Chem. Phys.* **1971**, *55*, 1811.
(54) Zunger, A.; Huler, E. *J. Chem. Phys.* **1975**, *62*, 3010.
(55) Mandell, M. J. *J. Low-Temp. Phys.* **1974**, *17*, 169.
(56) Raich, J. C.; Gillis, N. S. *J. Chem. Phys.* **1977**, *66*, 846.
(57) Weis, J.-J.; Klein, M. L. *J. Chem. Phys.* **1975**, *63*, 2869.
(58) Klein, M. L.; Weis, J.-J. *J. Chem. Phys.* **1977**, *67*, 217.
(59) Klein, M. L.; Lévesque, D.; Weis, J.-J. *J. Chem. Phys.* **1981**, *74*, 2566.
(60) Dolling, G. *Dynamics of Molecular Crystals*; Conference on Neutron Scattering, Gatlinburg, TN, 1976, p 263.
(61) Kiefte, H.; Clouter, M. J. *J. Chem. Phys.* **1976**, *64*, 1816.
(62) Press, W.; Janik, B.; Grimm, H. *Z. Phys. B: Condens. Matter* **1982**, *49*, 9.
(63) Sullivan, N. S.; Devoret, M.; Cowan, B. P.; Urbina, C. *Phys. Rev. B* **1978**, *17*, 5016.
(64) Nosé, S.; Klein, M. L. *Can. J. Phys.* **1985**, *63*, 1270.
(65) Ullo, J. J.; Yip, S. *Phys. Rev. Lett.* **1985**, *59*, 1509.
(66) Klee, H.; Carmesin, H. O.; Knorr, K. *Phys. Rev. Lett.* **1988**, *61*, 1855.
(67) Michel, J.; Drifford, M.; Rigny, P. *J. Chim. Phys.* **1970**, *67*, 31.
(68) Dolling, G.; Powell, B. M.; Sears, V. F. *Mol. Phys.* **1979**, *37*, 1859.
(69) Dove, M. T.; Pawley, G. S. *J. Phys. C: Solid State Phys.* **1983**, *16*, 5969.
(70) Dove, M. T.; Pawley, G. S. *J. Phys. C: Solid State Phys.* **1984**, *17*, 6581.
(71) Dove, M. T.; Powell, B. M.; Pawley, G. S.; Bartell, L. S. *Mol. Phys.* **1988**, *65*, 353.
(72) Dove, M. T.; Pawley, G. S.; Dolling, G.; Powell, B. M. *Mol. Phys.* **1986**, *57*, 865.
(73) Powell, B. M.; Dolling, G. *Can. J. Phys.* **1988**, *66*, 897.
(74) Maroncelli, M.; Qi, S. P.; Strauss, H. L.; Snyder, R. G. *J. Am. Chem. Soc.* **1982**, *104*, 6237. Maroncelli, M.; Strauss, H. L.; Snyder, R. G. *J. Chem. Phys.* **1985**, *82*, 2811.
(75) Ungar, G. *J. Phys. Chem.* **1983**, *87*, 689. Ungar, G.; Mašić, N. *J. Phys. Chem.* **1985**, *89*, 1036.
(76) Craievich, A. F.; Delonico, I.; Doucet, J. *Phys. Rev. B* **1984**, *30*, 4782. Strobl, G.; Ewen, B.; Fischer, E. W.; Piesczek, W. *J. Chem. Phys.* **1974**, *61*, 5257. Ewen, B.; Strobl, G.; Richter, D. *Faraday Discuss. Chem. Soc.* **1980**, *69*, 19.
(77) Taylor, M. G.; Kelusky, E. C.; Smith, I. C. P.; Casal, H. L.; Cameron, D. G. *J. Chem. Phys.* **1983**, *78*, 5108.
(78) Ryckaert, J.-P.; Klein, M. L.; McDonald, I. R. *Phys. Rev. Lett.* **1987**, *58*, 698.

(79) Ryckaert, J.-P.; McDonald, I. R.; Klein, M. L. *Mol. Phys.* **1989**, *67*, 957.
(80) Smith, A. E. *J. Chem. Phys.* **1953**, *21*, 2229.
(81) Ryckaert, J.-P.; Klein, M. L. *J. Chem. Phys.* **1986**, *85*, 1613.
(82) Ryckaert, J.-P.; Ciccotti, G. *Mol. Phys.* **1986**, *58*, 1125.
(83) Bloor, D.; Bonsor, D. H.; Batchelder, D. N.; Windsor, C. G. *Mol. Phys.* **1977**, *34*, 939. Doucet, J.; Dianoux, A. J. *J. Chem. Phys.* **1984**, *81*, 5043. Guillaume, F.; Doucet, J.; Sourisseau, C.; Dianoux, A. J. *J. Chem. Phys.* **1989**, *91*, 2555.
(84) Seymour, R. A.; Pryor, A. W. *Acta Crystallogr., Sect. B* **1970**, *28*, 1487.
(85) Garland, C. W.; Lushington, K. J.; Leung, R. C. *J. Chem. Phys.* **1979**, *71*, 3165.
(86) Klein, M. L.; McDonald, I. R.; Ozaki, Y. *J. Chem. Phys.* **1983**, *79*, 5579.
(87) Yamada, Y.; Noda, Y.; Axe, J. D.; Shirane, G. *Phys. Rev. B* **1974**, *9*, 4429.
(88) Nilsson, L.; Thomas, J. O.; Tofield, B. C. *J. Phys. C: Solid State Phys.* **1980**, *13*, 6441.
(89) Impey, R. W.; Klein, M. L.; McDonald, I. R. *J. Phys. C: Solid State Phys.* **1984**, *17*, 3941.
(90) Impey, R. W.; Klein, M. L.; McDonald, I. R. *J. Chem. Phys.* **1985**, *82*, 4690.
(91) Johansen, H. *Theor. Chim. Acta* **1973**, *32*, 273.
(92) Rahman, A. *J. Chem. Phys.* **1976**, *65*, 4845.
(93) Jacucci, G.; Rahman, A. *J. Chem. Phys.* **1978**, *69*, 4117.
(94) Chudley, C. T.; Elliot, R. S. *Proc. Phys. Soc. London* **1961**, *77*, 353.
(95) Aronsson, R.; Knape, H. E. G.; Torrell, L. W. *J. Chem. Phys.* **1982**, *77*, 677.
(96) Rowe, J. M.; Rush, J. J.; Chesser, N. J.; Michel, K. H.; Naudts, J. *Phys. Rev. Lett.* **1978**, *40*, 455.
(97) Lewis, L. J.; Klein, M. L. *Phys. Rev. Lett.* **1986**, *57*, 2698.
(98) Michel, K. H. *Phys. Rev. Lett.* **1986**, *57*, 2187; *Phys. Rev. B* **1986**, *35*, 1405, 1414.
(99) Michel, K. H. *Z. Phys. B: Condens. Matter* **1987**, *68*, 259.
(100) Bostoen, C.; Michel, K. H. *Z. Phys. B: Condens. Matter* **1988**, *71*, 45.
(101) Leutheusser, E. *Phys. Rev. A* **1984**, *29*, 2765. Bengtzelius, U.; Götze, W.; Sjölander, A. *J. Phys. C: Solid State Phys.* **1984**, *17*, 5915.
(102) Götze, W.; Sjögren, L. In *Dynamics of Disordered Materials*; Springer-Verlag: Berlin, 1989.
(103) Loidl, A. *Annu. Rev. Phys. Chem.* **1990**, *40*, 29.
(104) Rowe, J. M.; Hinks, D. G.; Price, D. L.; Susman, S.; Rush, J. J. *J. Chem. Phys.* **1973**, *58*, 2039.
(105) Rowe, J. M.; Rush, J. J.; Prince, E. *J. Chem. Phys.* **1977**, *66*, 5147.
(106) Rowe, J. M.; Rush, J. J.; Susman, S. *Phys. Rev. B* **1983**, *28*, 3506.
(107) Rowe, J. M.; Bouillot, J.; Rush, J. J.; Lüty, F. *Physica (Amsterdam)* **1986**, *136B*, 498.
(108) Knorr, K.; Loidl, A. *Phys. Rev. B* **1985**, *31*, 5387.
(109) Knorr, K.; Loidl, A.; Kjems, J. K. *Phys. Rev. Lett.* **1985**, *55*, 2445.
(110) Rowe, J. M.; Rush, J. J.; Hinks, D. G.; Susman, S. *Phys. Rev. Lett.* **1979**, *43*, 1158.
(111) Volkmann, U. G.; Böhmer, B.; Loidl, A.; Knorr, K.; Höchli, U. T.; Haussühl, S. *Phys. Rev. Lett.* **1986**, *56*, 1716.
(112) Doverspike, M. A.; Wu, M.-C.; Conradi, M. S. *Phys. Rev. Lett.* **1986**, *56*, 2284.
(113) Impey, R. W.; Klein, M. L.; Sprik, M. *J. Chem. Phys.* **1985**, *83*, 3638.
(114) Bounds, D. G.; Klein, M. L.; McDonald, I. R. *Phys. Rev. Lett.* **1981**, *46*, 1682.
(115) Klein, M. L.; McDonald, I. R. *Chem. Phys. Lett.* **1981**, *78*, 383.
(116) Klein, M. L.; McDonald, I. R. *J. Chem. Phys.* **1983**, *79*, 2333.
(117) Impey, R. W.; Nosé, S.; Klein, M. L. *Mol. Phys.* **1983**, *50*, 243.
(118) Ferrario, M.; McDonald, I. R.; Klein, M. L. *J. Chem. Phys.* **1986**, *84*, 3975.
(119) Lewis, L. J.; Klein, M. L. *J. Phys. Chem.* **1987**, *91*, 4990.
(120) Lewis, L. J.; Klein, M. L. *Phys. Rev. Lett.* **1987**, *59*, 1837.
(121) Lewis, L. J.; Klein, M. L. *Phys. Rev. B* **1989**, *40*, 4877.
(122) Lewis, L. J.; Klein, M. L. *Phys. Rev. B* **1989**, *40*, 7080.
(123) Lewis, L. J.; Klein, M. L. *Phys. Rev. B* **1989**, *40*, 7904.
(124) Edwards, S. F.; Anderson, P. W. *J. Phys. F: Met. Phys.* **1975**, *5*, 965.
(125) Bounds, D. G.; Klein, M. L.; McDonald, I. R.; Ozaki, Y. *Mol. Phys.* **1982**, *47*, 629.
(126) Smith, W.; Clarke, J. H. R. *J. Chem. Phys.* **1989**, *90*, 6647.
(127) Lynden-Bell, R. M.; Ferrario, M.; McDonald, I. R.; Salje, E. *J. Phys.: Condens. Matter* **1989**, *1*, 6523.
(128) Grimsditch, M.; Torell, L. M. In *Dynamics of Disordered Materials*; Springer-Verlag: Berlin, 1989; *Phys. Rev. Lett.* **1989**, *62*, 2616.
(129) Howell, F. S.; Bose, R. A.; Macedo, P. B.; Moynihan, C. T. *J. Phys. Chem.* **1979**, *78*, 639.
(130) Weiler, R.; Bose, R. A.; Macedo, P. B. *J. Chem. Phys.* **1970**, *53*, 1258. Dietzel, A.; Poegel, H. P. In *Proceedings of the Third International Glass Congress*, Venice, 1963.
(131) Torell, L. M. *J. Chem. Phys.* **1983**, *78*, 1121. Angell, C. A.; Torell, L. M. *J. Chem. Phys.* **1983**, *78*, 937.
(132) Signorini, G. F.; Barrat, J.-L.; Klein, M. L. *J. Chem. Phys.* **1990**, *92*, 1294.
(133) Kirkpatrick, T. R.; Thirumalai, D.; Wolynes, P. G. *Phys. Rev. A* **1989**, *40*, 1045 and references therein.
(134) Mezei, F.; Knaak, W.; Farago, B. *Europhys. Lett.* **1988**, *7*, 529.
(135) Richter, D.; Frick, B.; Farago, B. *Phys. Rev. Lett.* **1988**, *61*, 2465.
(136) Knaak, W.; Mezei, F.; Farago, B. *Phys. Rev. Lett.* **1987**, *58*, 571. Mezei, F.; Knaak, W.; Farago, B. *Phys. Scr.* **1987**, *T19*, 363.
(137) Bernu, B.; Hansen, J.-P.; Hiwatari, Y.; Pastore, G. *Phys. Rev. A* **1987**, *36*, 4891. Pastore, G.; Bernu, B.; Hansen, J.-P.; Hiwatari, Y. *Phys. Rev. A* **1988**, *38*, 454.
(138) Roux, J.-N.; Barrat, J.-L.; Hansen, J.-P. *J. Phys.: Condens. Matter* **1989**, *1*, 7171.
(139) Ullo, J. J.; Yip, S. *Phys. Rev. A* **1989**, *39*, 5877.
(140) Angell, C. A.; Clarke, J. H. R.; Woodcock, L. V. *Adv. Chem. Phys.* **1981**, *48*, 397. Frederickson, G. H. *Annu. Rev. Phys. Chem.* **1988**, *39*, 149.
(141) Ivanov, E. N. *Sov. Phys.* **1964**, *18*, 1041; *J. Exptl. Theor. Phys. (USSR)* **1963**, *45*, 1509.
(142) Clarke, J. H. R.; Miller, S. *Chem. Phys. Lett.* **1972**, *13*, 97.
(143) Cheng, L.-T.; Yan, Y.-X.; Nelson, K. A. *J. Chem. Phys.* **1988**, *88*, 6477; **1989**, *91*, 6052.